

OPTIMIZATION OF THE SLAG TAP FOR THE GASIFICATION OF
SUSTAINABLE FEEDSTOCKS

A THESIS IN
Mechanical Engineering

Presented to the Faculty of the University
of Missouri-Kansas City in partial fulfillment of
the requirements of the degree

MASTER OF SCIENCE

by

NOAH AVRAM MELTZ WEICHSELBAUM

B.S., Union College, 2006

Kansas City, Missouri

2011

© 2011

NOAH AVRAM MELTZ WEICHSELBAUM

ALL RIGHTS RESERVED

OPTIMIZATION OF THE SLAG TAP FOR THE GASIFICATION OF
SUSTAINABLE FEEDSTOCKS

Noah Avram Meltz Weichselbaum, Candidate for the Master of Science Degree

University of Missouri-Kansas City, 2011

ABSTRACT

The objective of this study was to optimize a slag tapping block for use with a molten slag bath containing slag from the gasification of biomass and municipal solid waste feedstocks. Theoretical testing was conducted on the slag tapping block implementing computational fluid dynamics and design of experiments. It was desired to see how factors affecting the slag tap could be optimized to result in the minimum required temperature of the slag bath to reduce costs associated with auxiliary means of heating the slag bath.

The faculty listed below, appointed by the Dean of the School of Computing and Engineering have examined a thesis titled “Optimization of the Slag Tap for the Gasification of Sustainable Feedstocks,” presented by Noah A. M. Weichselbaum, candidate for the Master of Science degree, and certify that in their opinion it is worthy of acceptance.

Supervisory Committee

Anthony F. Black, Ph.D., Advisor
School of Computing and Engineering

Gregory W. King, Ph.D., Committee Chair
School of Computing and Engineering

Bryan R. Becker, Ph.D.
School of Computing and Engineering

Amber Stern, Ph.D.
School of Computing and Engineering

CONTENTS

ABSTRACT	iii
LIST OF ILLUSTRATIONS.....	vii
LIST OF TABLES.....	ix
ACKNOWLEDGEMENTS.....	x
Chapte	
1. INTRODUCTION	1
2. REVIEW OF LITERATURE	5
3. METHODOLOGY.....	8
3.1 Overview.....	8
3.2 Model Creation	9
3.3 Model Simulation	20
3.4 Design of Experiments.....	23
4. RESULTS	25
4.1 Water Cooling Channel Simulation.....	25
4.2 Specific Heat and Thermal Conductivity.....	27
4.3 Viscosity Simulation.....	30
4.4 Model Simulation	32
4.5 Design of Experiments.....	45
5. DISCUSSION	58
5.1 Model Simulation	58

5.2 Future Work.....	62
5.3 Conclusion.....	63
Appendix	
A. Interpreted Viscosity Equations for Fluent.....	64
B. Heat Transfer Coefficient for Copper Pipe.....	66
C. Heat Transfer Coefficient for Steel Wall	68
D. 2 ³ Factorial Design Output	70
E. Auxiliary Heating Cost Calculation for Various Feedstocks	76
F. Polynomial Equations for Specific Heat and Thermal Conductivity	80
REFERENCE LIST	90
VITA	92

ILLUSTRATIONS

Figure		Page
1.	Slag Tapping Block Model Layout.....	10
2.	Model Inlet Named Selections	12
3.	Internal Water Cooling Channels.....	13
4.	Model Outlet Named Selections	15
5.	Pressure-Based Segregated Algorithm.....	22
6.	Energy Absorbed by Water Cooling Channels	26
7.	Slag Viscosity versus Temperature.....	32
8.	Temperature and Viscosity Contours for Coal Slag for Minimum Diameter and Minimum Length.....	33
9.	Temperature and Viscosity Contours for Coal Slag for Maximum Diameter and Minimum Length.....	34
10.	Temperature and Viscosity Contours for Coal Slag for Minimum Diameter and Maximum Length	35
11.	Temperature and Viscosity Contours for Coal Slag for Maximum Diameter and Maximum Length	36
12.	Temperature and Viscosity Contours for Biomass Slag for Minimum Diameter and Minimum Length.....	37
13.	Temperature and Viscosity Contours for Biomass Slag for Maximum Diameter and Minimum Length.....	38
14.	Temperature and Viscosity Contours for Biomass Slag for Minimum Diameter and Maximum Length	39
15.	Temperature and Viscosity Contours for Biomass Slag for Maximum Diameter and Maximum Length	40
16.	Temperature and Viscosity Contours for MSW Slag for Minimum Diameter and Minimum Length.....	41

17.	Temperature and Viscosity Contours for MSW Slag for Maximum Diameter and Minimum Length.....	42
18.	Temperature and Viscosity Contours for MSW Slag for Minimum Diameter and Maximum Length.....	43
19.	Temperature and Viscosity Contours for MSW Slag for Maximum Diameter and Maximum Length.....	44
20.	Main Effects Plots for Slag Bath Temperatures.....	48
21.	Cube Plots (data means) for Slag Bath Temperatures	49
22.	Interaction Plots for Slag Bath Temperatures	50
23.	Pareto Charts for the Standardized Effects for Slag Bath Temperatures ...	52
24.	Normal Probability Plots for Slag Bath Temperatures	54
25.	Versus Fits for Slag Bath Temperatures	55
26.	Response Optimizer for Slag Bath Temperatures.....	57

TABLES

Table	Page
1. Elemental Analysis of Slag	17
2. 2^3 Factorial Design Method	23
3. Specific Heat and Thermal Conductivity Coefficients for Fluent	28
4. Viscosity Groupings and Constants	31
5. Factorial Design Data.....	45

ACKNOWLEDGEMENTS

There are many people who deserve thanks for supporting me or leading me to accomplish this.

First and foremost I have to thank my Advisor, Dr. Anthony Black, for providing this excellent opportunity. I look forward to continuing research in this field, and continuing to better myself and contributing to the advancement of knowledge in this industry.

I also would like to thank my committee, Dr. Gregory W. King and Dr. Bryan R. Becker for their help and support. Last I would like to thank my fiancé Natasha and my parents Paul and Elyse for their continued support through this process.

CHAPTER 1

INTRODUCTION

Gasification is an energy producing process that is clean and efficient, and can make use of varying feedstocks including coal, petroleum coke, biomass, heavy oil, and municipal solid waste. One of the byproducts from the gasification of fuels is slag that is composed of inorganic matter. In gasifiers where the vessel temperature is greater than the ash fusion temperature, the inorganic fraction containing heavy metals will melt and form a liquid slag. One method of slag removal is through a slag bath that is equipped with a tapping mechanism. Through optimizing the slag tap for the gasification process it is believed that the cost associated with the auxiliary heating of the slag bath can be reduced.

Gasification is a process by which the feedstock containing carbonaceous materials is partially oxidized, or partially combusted, creating a synthesis gas (syngas) consisting of H_2 and CO that is suitable for use in combustion turbines. Syngas is an ideal fuel when utilized in a combustion turbine since it can drastically lower emissions compared to the combustion of coal. This is due to the reduced stoichiometric oxygen-to-fuel ratio in gasification that can be up to four times less than what is required for complete oxidation in combustion processes. Emissions from fuel bound nitrogen and sulfur that through combustion are converted to NO_x and SO_x , are instead converted to N_2 , NH_3 , and HCN for nitrogen, and H_2S and COS for sulfur. The syngas can then be used to power turbines in an integrated gasification

combined cycle (IGCC) where the emissions would be significantly less when compared with a conventional coal fired power plant.

The methods of gasification can be classified through three main types of gasifiers; entrained flow, fluidized bed, and moving bed. In entrained flow gasifiers, finely divided feedstock is fed in co-current flow with the oxidant at high temperature that raise the ash produced above the ash fusion temperature resulting in slagging operation. The residence time in an entrained flow gasifier is extremely brief as the feedstock rapidly heats up and reacts with the oxidant. This requires that the feedstock be homogenous which makes this type of gasifier unsuitable for biomass or MSW which cannot be readily pulverized. Fluidized bed and moving bed gasifiers operate at lower temperatures making them more suitable for biomass and MSW feedstocks. The fluidized bed gasifier is defined by a reactor in which new feedstock particles are mixed with partially and fully gasified particles. The flow of gas into the reactor is just enough to suspend the feedstock particles. However, fluidized bed gasifiers are non-slagging, for if the ash fusion temperature is exceeded it would cause agglomeration that would result in the bed de-fluidizing. The moving bed gasifier operates through a counter current flow of oxygen and steam introduced through tuyeres in the sides of the vessel in the combustion zone that moves up through the reactor vessel while the feedstock is fed through a lock hopper at the top of the vessel. The feedstock descends through three zones beginning with upper zone where the feedstock is dried and devolatilized, in the next zone it is gasified, and in the last zone it is combusted. The remaining ash content of the feedstock can either be dry or it can be liquefied forming slag that flows down into the slag bath.

The slag bath is typically contained in a vessel with a refractory wall that is water cooled. For this research the primary area of interest is the extraction method of the slag from the slag bath. There are numerous methods for removal of slag from the slag bath, this research focuses on biomass and MSW feedstock that would be utilized in a moving bed gasifier and extracted through a side tap located near the bottom of the slag bath.

The capital cost of an IGCC is significantly more than the cost of a conventional coal fired plant with environmental protection, and the reliability is less (Department of Trade and Industry 1998). However, the numerous benefits of gasification make research and development valuable. Gasification allows for greater variety of fuel sources, and when MSW feedstock is utilized it reduces the amount of MSW being sent to incinerators and landfills reducing the negative impact on the environment. Gasification of coal feedstock can also reduce landfill waste, IGCC bottom slag has a low loss on ignition (LOI) and is non-leachable making it usable for construction materials, road de-icing grit, and sand blasting. The bottom ash from a pulverized coal boiler typically has a higher LOI and is leachable. This requires that the ash be sent to special landfills that are carefully designed to minimize the risk of groundwater contamination from the chemicals in the ash, this can add a significant cost to the coal fired plant system.

The tap for the slag bath plays a critical part in addressing concerns with the gasification process, both from a financial aspect as well as reliability. A well designed, and efficient, slag tapping system and bath, can help to reduce the capital cost of the gasification plant through reduced material costs and footprints for the

plant. A robust design of the tap will also help with operation and maintenance costs, as it will have an optimized life for performance and will minimize risks of clogging. A typical quench type slagging gasifier collects 7.5 tons/hour (Buttker et al. 2005) of slag, so a dysfunctional slag tap can have extremely detrimental effects on plant operation even leading to plant shutdown. Through optimized design of the tapping system, the concern with reliability of the gasification system in this area can be addressed, making the overall system more competitive with coal fired plants both in reliability and cost.

CHAPTER 2

REVIEW OF LITERATURE

Slag is an important part of the gasification process that requires research into how it affects critical parts of the gasifier such as refractory walls and taps. The physical properties of slag and the temperature it is maintained at throughout the gasification process can cause problems due to its reactive nature towards refractory walls and maintaining adequate viscosities for flow through taps. The advent of Computation Fluid Dynamics (CFD) modeling has made it possible to approximate values for how slag properties react during the gasification process and develop designs to rectify these issues. Slag properties can change significantly when design variables including bath temperature, feedstock material, and tapping block geometries are altered.

In order to properly model slag in CFD analyses, the properties of the slag must be accurate. Research into the properties for characterizing slag has been advanced and documented furthest by the work of Mills (Mills 2011) and Vargas (Vargas et al. 2000). Their studies have developed means for characterizing such properties as viscosity and thermal conductivity of liquid slags in relation to temperature. Mills and Vargas tested and researched many of the mathematical models for determining properties of slag from their peers to determine which types of slag would be applicable and the percent error in these models approximation. One of their peers, Urbain, prepared in a lab 60 different compositions of ternary SiO_2 -

Al_2O_3 -MO and SiO_2 - Al_2O_3 - M_2O mixtures to work out models for the estimation of the viscosity of ceramics (Vargas et al. 2000). This made possible future applications of this mathematical model to characterizing the viscosity of molten silicate slags through the defining the oxides present in the slag.

There have been many studies conducted on the gasification process employing CFD analysis that have enhanced understanding of how slag flow and slag taps can affect gasifiers. One such study by Wang (Wang et al. 2007) was a CFD analysis on a quench type coal gasifier in the Southern Taiwan City of Kaohsiung. This analysis was prompted by actual problems with the slag tap at the bottom of the gasifier clogging when converting pulverized coal and petroleum cokes into syngas. Wang's (Wang et al. 2007) CFD analysis modeled the chemical reactions of coal gasification in addition to volatile combustion to determine how widening of the slag tap to avoid clogging would affect thermal efficiency and gasifier performance. Another study by Ashrafian and Johansen (Ashrafian and Johansen 2006) conducted research into side tapping of molten metal and slag from a coke-bed in a furnace hearth. A 2-D CFD analysis was implemented to determine how the behavior and motion of the liquid to liquid interface during tapping could be affected by the density and viscosity of the fluids in addition to the presence of a packed bed.

This research focuses on the slag tap and isolates the slag tap in a "black box" from the rest of the gasification process. The process outside of the "black box" is accounted for through use of material and thermal boundary conditions. In Wang's (Wang et al. 2007) research slagging was not modeled and although Ashrafian and Johansen (Ashrafian and Johansen 2006) modeled the slag it was estimated with

constant values for molten metals from the Slag Atlas. Moving forward this research proposes to use thermal property characterizations for slag developed by Mills (Mills 2011) and Vargas (Vargas et al. 2000) integrated into a CFD analysis to model the slag flow through the slag tap. This research will also focus on biomass slag from Lignocellulose fermentation and municipal solid waste slag, where the studies by Wang (Wang et al. 2007) and Ashrafian and Johansen (Ashrafian and Johansen 2006) were on coal slag which has been studied much more thoroughly.

This research affords the ability to better understand the slag flow in the tapping region that is believed to be an integral part of the gasification process. Through Design of Experiments (DOE) optimization this research will determine the ideal geometry for the slag tap and slag flow rate to be able to maintain the lowest slag bath temperature reducing auxiliary heating costs while not clogging the tap. There are concerns over the reliability and costs associated with gasification plants and as this applies to the slag tap this research could help mitigate these concerns in this area.

CHAPTER 3

METHODOLOGY

3.1 Overview

Gasification of sustainable feedstocks such as biomass and municipal solid waste (MSW) is an area that requires research into the physical properties of the slag to properly design components of the gasification system. This research focused on the slag tapping component of the system, and presents a novel way for characterizing the material properties of the slag so that the viscosity can be adequately modeled in the slag channel.

It is critical that the viscosity of the slag be maintained in a range of 8-15 (Pascal*seconds) to avoid crystallization of the slag in the tapping channel (Van Der Drift et al. 2003). This research assumed that all of the slag obeyed Newton's law of viscosity, and the lower limit of 8 (Pa*s) was maintained in all analyses to ensure this.

The simulation of the slag channel was conducted utilizing the CFD software package ANSYS Fluent. CFD was integral to this research due to the need for a complete fluid profile of the slag within the tapping channel to ensure the viscosity remained below the set limit at all points within the channel. This particular software package was chosen due to its ability to model species transport without reactions. The method used for characterizing the liquid slag was to utilize existing elemental

analyses of biomass, MSW, and coal slags that defined the species mol fractions of the metal oxides constituting the fluid. These species mol fractions were implemented into CFD in addition to a method for characterizing the specific heat, thermal conductivity, and viscosity of the slag as functions of temperature.

The CFD model was then used to determine what the minimum inlet temperature of the slag bath could be in order to maintain the viscosity limits throughout the tapping channel. Through calculating the minimum bath temperature, a cost could be determined for the auxiliary heating of the slag bath. Various factors affecting the slag tap were then varied to determine the optimized design of the slag tapping channel. A DOE 2^k factorial method was implemented to determine the optimal design for the cost of heating the slag bath.

3.2 Model Creation

The model of the slag tapping block was created in Autodesk Inventor (Figure 1). The model did not define the entire slag bath, modeling the entire system would consume computing resources that for this research was better allocated to refined meshes on the surfaces of the slag channel. Through refining the mesh on the fluid region containing the slag more accurate results were obtained for the viscosity of the slag and problems with convergence were avoided. The rest of the slag bath system was represented through thermal boundary conditions.

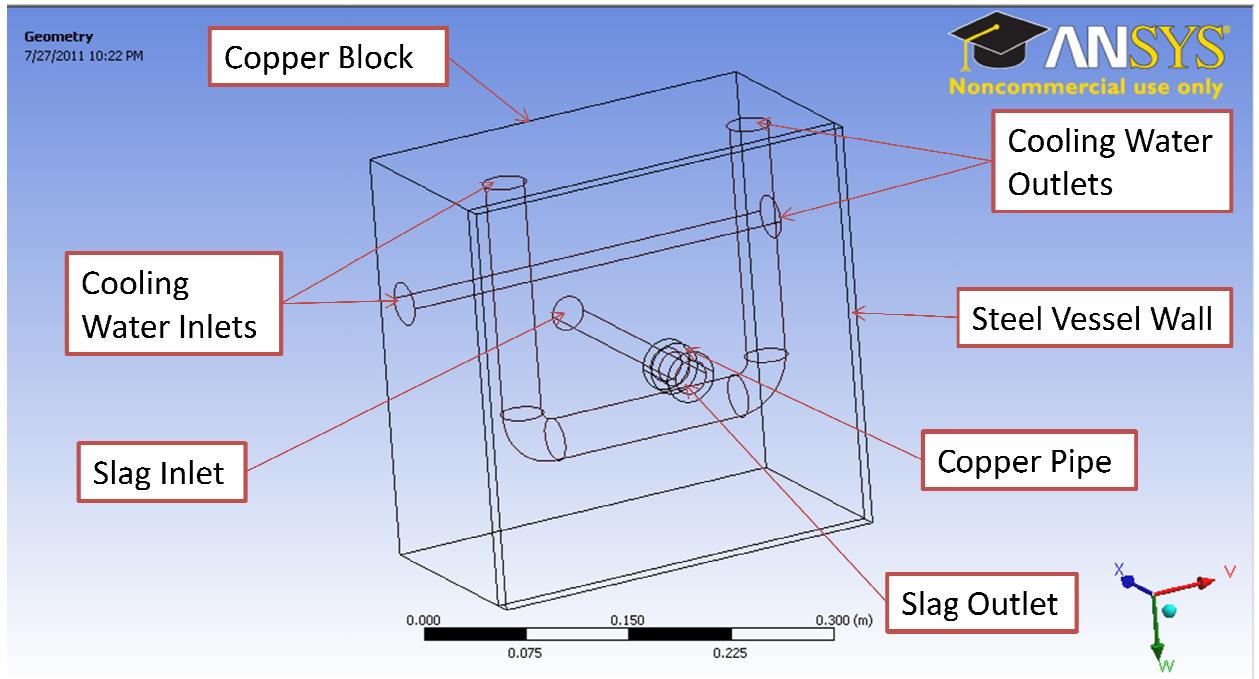


Figure 1. Slag Tapping Block Model Layout

The model in Figure 1 represents a typical tapping block that would be used for the tapping of slag from a slag bath. The copper block has two water cooling channels for maintaining the temperature of the copper block, and the slag channel runs through the center of the block. The copper pipe for the slag then runs from the block, through the steel vessel wall to atmosphere where the slag is discharged.

The model was loaded from Autodesk Inventor into the ANSYS Workbench where the mesh was applied and bodies and faces were named for use in CFD. These named selections were used in CFD to define the different material properties for bodies, and the different thermal boundary conditions for the faces, both of these aspects of the model were important criteria for creating an accurate model. The

copper block was detailed first defining the thermal boundary conditions and material properties.

The copper block's material properties were defined using the CFD program's material properties database. The inlet face of the copper block (Figure 2) was named "Copper Wall Exposed to Slag" and was designated as a heat flux thermal boundary condition that represents the heat transfer from the slag bath with a heat flux of 88 (Watts/meter²) (Featherston 2003). The slag from the slag bath entered the copper block at the face named "Inlet" that was set as a velocity inlet boundary condition. This boundary also defined the temperature of the slag bath and the composition of the species of metal oxides that made up the slag. The other four faces of the copper block were named "Copper Wall" and were considered to be exposed entirely to the refractory wall, these walls did not have a temperature profile, but were set as adiabatic walls with a heat flux of zero.

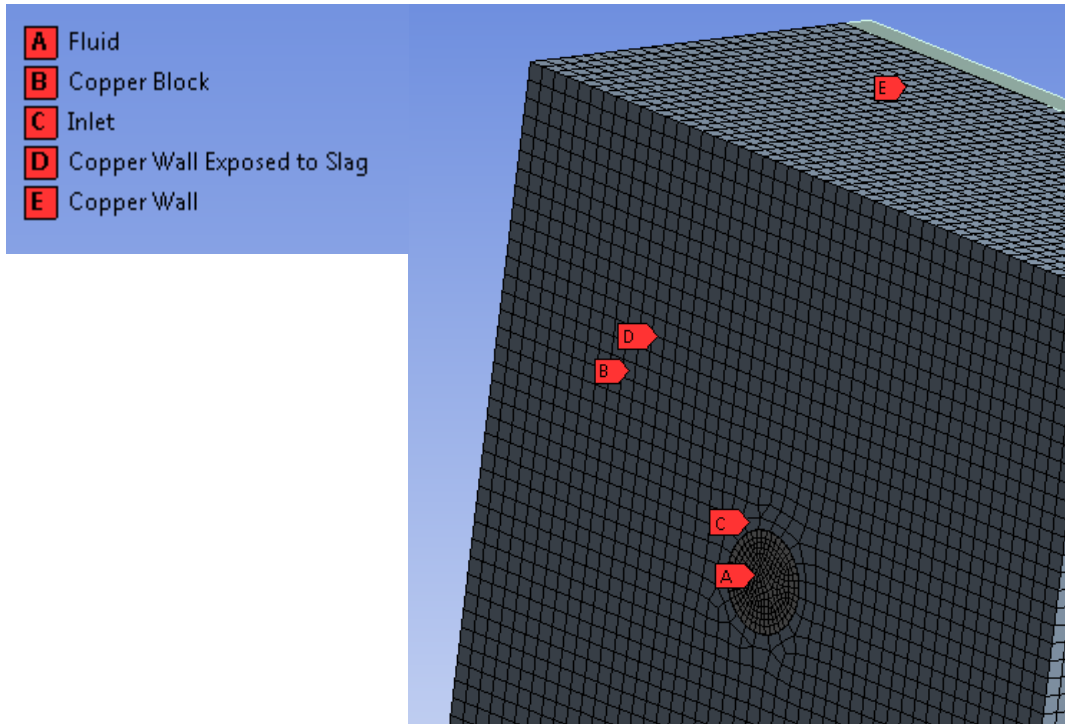


Figure 2. Model Inlet Named Selections

The copper block is typically fitted with internal water cooling channels to maintain the block at an acceptable operational temperature. Ideally these water channels would be modeled in the CFD analysis, however, since species transport was being used to define the liquid slag, other fluid materials were not allowed to be specified in this analysis (ANSYS 2010). To represent the water cooling channels the material properties of the solid copper was given the property of an energy term in Watts per meter cubed that defined the amount of heat removed by the internal water channels. The value for this term was determined by conducting a separate CFD

analysis with an identical geometrical setup (Figure 2), plus the addition of internal water channels (Figure 3).

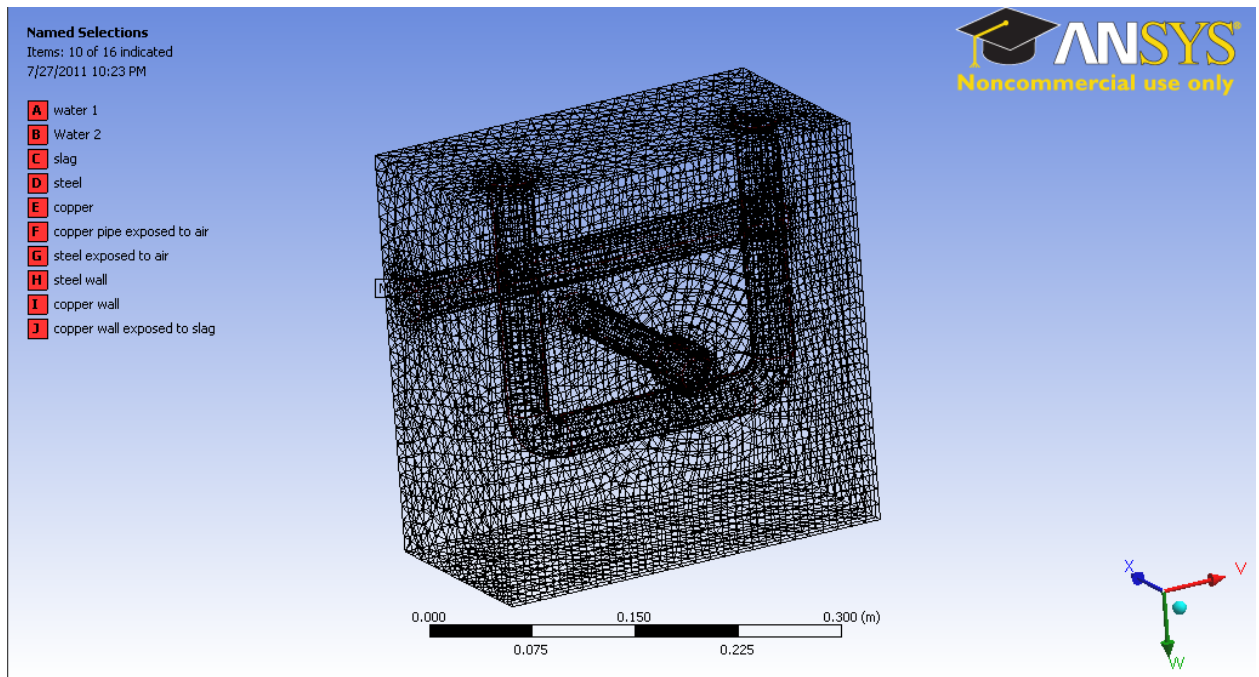


Figure 3. Internal Water Cooling Channels

The properties of the internal water cooling channels were determined from a study on tapping block designs for copper smelters (Feathersont) to be 2.25 (Liter/second) for each channel with a fixed inlet temperature of 27 degrees Celsius. Since this model could not be used with the actual slag mixture, the dominant species of the slag being analyzed was used to approximate the fluid. The other thermal

boundary conditions were maintained with the same properties as the species transport analysis.

The energy absorbed by the water was solved for in Fluent and a polynomial equation relating energy absorbed to temperature was created. This value was integrated into the species transport model to represent the heat absorbed from the water cooling channels.

The discharge of the slag from the copper block goes through a copper pipe that extends through the steel vessel wall into atmospheric conditions (Figure 4). The copper pipe was defined with the same material properties as the block but with no water cooling energy source terms. The region of the copper pipe embedded in the steel wall had a thermally coupled boundary condition. The surfaces of the pipe that extended past the steel wall had a mixed convection and radiation heat transfer coefficient (Appendix B). The outlet for the slag to atmospheric conditions was defined as a pressure outlet with atmospheric temperature.

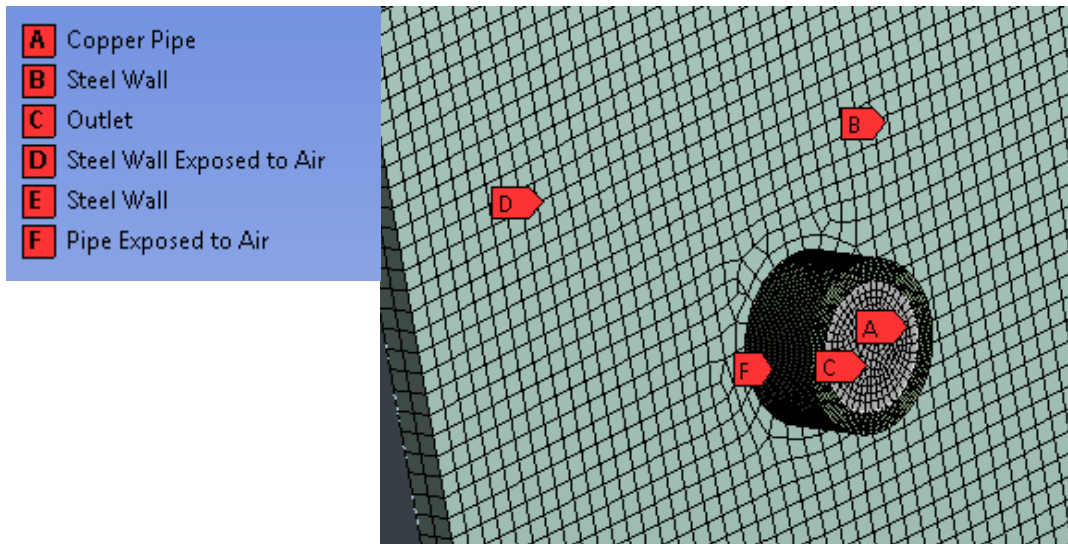


Figure 4. Model Outlet Named Selections

The “Steel Wall” had material properties defined by the CFD program material’s database, and it had both a thermally coupled boundary condition with the copper pipe as well as the copper block. The face named “Steel Wall Exposed to Air” had a mixed convection and radiation thermal boundary condition (Appendix C). This type of thermal boundary condition was implemented because it represented the rate of heat loss from the wall due to natural convection and radiation that occurred due to the temperature variation between the wall and the air at atmospheric temperature. The other four surfaces were grouped together and named “Steel Wall” and these surfaces were considered to be adiabatic with a heat flux of zero.

The “fluid” body (Figure 4) is the region that represents the liquid slag. The composition of the slag was determined from the elemental analysis of slag for

biomass (Blunk and Jenkins 2000), MSW (Zhan et al. 2009), and coal (Ilyushechkin et al. 2010). The material properties for each oxide were defined either through constant values from the NIST Chemistry Webbook and Lide (Lide 2005), or polynomial functions. The constant values, the oxides that constitute the respective slag, and the mol fractions can be seen in Table 1. These compositions have a direct effect on the physical and mechanical properties of the slag, therefore it was determined this would be an appropriate way to model the liquid slag region in Fluent.

Table 1. Elemental Analysis of Slag

Slag	Oxide	Mol Fraction	Density (kg/m ³)	Molecular Weight
Coal	SiO ₂	0.495	2211	60.085
	Al ₂ O ₃	0.207	3986	101.96
	TiO ₂	0.012	4230	79.566
	Fe ₂ O ₃	0.199	5242	159.69
	CaO	0.037	3350	56.08
	MgO	0.025	3580	40.3
	Na ₂ O	0.024	2270	61.98
	K ₂ O	0.002	2350	94.2
Biomass	SiO ₂	0.183	2211	60.085
	Al ₂ O ₃	0.036	3986	101.96
	TiO ₂	0.003	4230	79.566
	Fe ₂ O ₃	0.016	5242	159.69
	CaO	0.234	3350	56.08
	MgO	0.056	3580	40.3
	Na ₂ O	0.016	2270	61.98
	K ₂ O	0.173	2350	94.2
	P ₂ O ₅	0.279	2390	141.944
So ₃	0.004	1920	80.063	
MSW	SiO ₂	0.537	2211	60.085
	Al ₂ O ₃	0.126	3986	101.96
	TiO ₂	0.013	4230	79.566
	Fe ₂ O ₃	0.079	5242	159.69
	CaO	0.167	3350	56.08
	MgO	0.024	3580	40.3
	Na ₂ O	0.043	2270	61.98
	K ₂ O	0.011	2350	94.2

Two other material properties that were defined were the specific heat and the thermal conductivity of each material. Coefficients for each individual metal oxide were found from the NIST Chemistry Webbook that formed temperature dependent properties for specific heat and thermal conductivity. These coefficients fit into a function that was defined as:

$$C_p = A + B * \left(\frac{t}{1000}\right) + C * \left(\frac{t}{1000}\right)^2 + D * \left(\frac{t}{1000}\right)^3 + E / \left(\frac{t}{1000}\right)^2 \quad (1)$$

Where C_p is the specific heat (Joule/mol*Kelvin), and T is the temperature (K). The polynomial equation that is embedded in the CFD program for temperature dependant properties has the function defined as

$$C_p = A + B * t + C * t^2 + D * t^3 + E * t^4 \quad (2)$$

The coefficients for use with Equation 1 were used to generate curves of the specific heat as a function of temperature in Microsoft Excel. Regression analysis was then implemented to determine a new function that would fit the format of Equation 2.

The equation for thermal conductivity (Incropera 2002) was dependent on the value for specific heat and was defined as:

$$k = \alpha * c_p \quad (3)$$

Where k is the thermal conductivity (W/m*K), and α is the thermal diffusivity that was found to be independent of temperature, and to have an approximate value of $4.5e-7$ (m²/s) (Mills and Rhine 1989).

Viscosity was the last material property defined. Similar to the specific heat and the thermal conductivity, the viscosity was defined with a temperature dependant equation that was based on the Urbain model for viscosity (Vargas et al. 2000). The

Urbain model was the result of an empirical fitting of data relating viscosity to temperature, and it only applied to Newtonian liquids. The first step in the Urbain process was to group the species that constituted the slag as glass formers, glass modifiers, and glass amphoteric. The following functions defined these groups

$$x_g = SiO_2 + P_2O_5 \quad (4)$$

$$x_m = FeO + CaO + MgO + Na_2O + K_2O + MnO + NiO + 2 * (TiO_2 + ZrO_2) + 3 * CaF_2 \quad (5)$$

$$x_a = Al_2O_3 + Fe_2O_3 + B_2O_3 \quad (6)$$

The groups for glass modifiers and glass amphoteric were then used to calculate the constant alpha defined as:

$$\alpha = \frac{x_m}{x_m + x_a} \quad (7)$$

Constants b could then be calculated based on the value of alpha and the molar ratio of SiO₂.

$$b_0 = 13.8 + 39.9355 * \alpha - 44.049 * \alpha^2 \quad (8)$$

$$b_1 = 30.481 - 117.1505 * \alpha + 129.9978 * \alpha^2 \quad (9)$$

$$b_2 = -40.9429 + 234.0486 * \alpha - 300.04 * \alpha^2 \quad (10)$$

$$b_3 = 60.7619 - 153.927 * \alpha + 211.161 * \alpha^2 \quad (11)$$

$$b = b_0 + b_1 * SiO_2 + b_2 * SiO_2^2 + b_3 * SiO_2^3 \quad (12)$$

Constants for b and alpha were then utilized to find the parameter a in (Pa*s/K) using the function defined as:

$$-ln * a = 0.2693 * b + 13.9751 \quad (13)$$

A formula for the viscosity as a function of temperature was determined based on the Weyman formula (Vargas et al. 2000) and could be expressed as:

$$\eta = a * T * \exp\left(\frac{1000*b}{T}\right) \quad (14)$$

Where η is the viscosity (Pa*s) and a and b were determined in equations 12 and 13 respectively. Equation 14 was then written in C code (Appendix A) for each type of slag, and interpreted as a user defined function into CFD to be utilized for the viscosity material property.

3.3 Model Simulation

In order to optimize the system, factors effecting the bath temperature were identified and a range for each factor was determined. The factors chosen were the length of the copper block, the diameter of the channel for the slag, and the velocity of the slag flow.

The maximum and minimum value for each factor was analyzed in CFD in separate runs for each feedstock material. There were twenty-four sets of analyses run in CFD for the three types of material and the varying factors. Each individual analysis was run to convergence for varying slag bath temperatures. This temperature was varied until the minimum temperature was found that would still result in a fluid profile that did not exceed a viscosity of 8 (Pa*s) at any point in the fluid region.

CFD was integral in being able to determine the fluid profile of the slag within the tapping channel for both the temperature and the viscosity of the fluid. The flow of the slag was assumed to behave as an incompressible flow. The slag flow was also found to be laminar from the following function:

$$Re = \frac{DV\rho}{\mu} \quad (15)$$

Where D is the diameter of the slag tap, V is the inlet velocity of the slag, ρ is the density of the slag, and μ is the viscosity. The unitless number for the Reynold's number was checked in the different analysis results and was found to be well below the limit for laminar flow of 2000.

The pressure-based segregated solver was used for the analysis in CFD (Figure 5).

Pressure-Based Segregated Algorithm

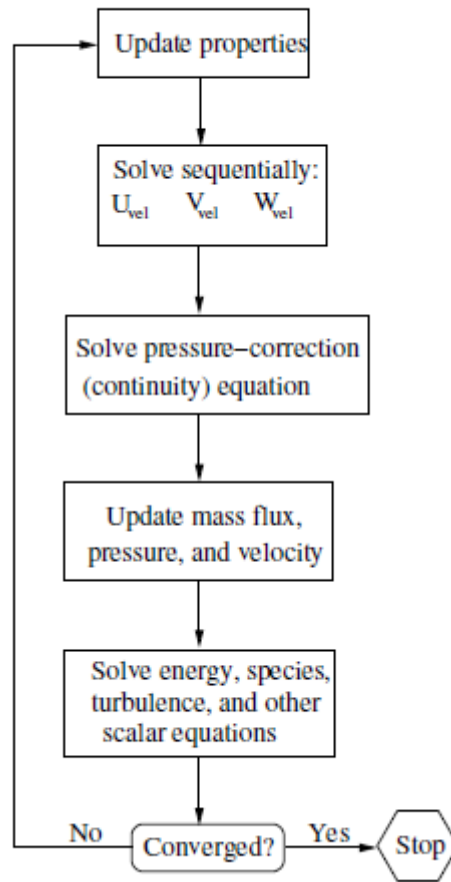


Figure 5. Pressure-Based Segregated Algorithm

Where the governing equations were solved sequentially. The equations being solved were the mass conservation, momentum conservation, energy conservation, and species transport equations. All of the equations were solved using a second order upwind discretization scheme.

These equations were non-linear and segregated from each other while the solution was being solved. These equations were carried out iteratively until the scaled residual of the final solution was reduced to 10^{-6} of the initial residual which was the convergence criteria.

3.4 Design of Experiments

The ideal combinations of maximum and minimum values for the diameter of the tap, length of the tap, and velocity of the slag were determined by a 2^3 factorial design method (Table 4) that was implemented for each slag material. These combinations of factors in the context of DOE are referred to as treatments. The 2^3 full factorial design was selected due to its ability to investigate all of the individual factors and their interactions with the minimum number of treatments. The -1 represents the coded first level of the factor and the 1 represents the second level.

Table 2. 2^3 Factorial Design Method

Treatment Name	Factors		
	A	B	C
(1)	-1	-1	-1
a	1	-1	-1
b	-1	1	-1
ab	1	1	-1
c	-1	-1	1
ac	1	-1	1
bc	-1	1	1
abc	1	1	1

This type of method produces a linear model for determining the response that has a linear regression function of:

$$y = B_0 + B_1x_1 + B_2x_2 + B_{12}x_1x_2 + B_3x_3 + B_{13}x_1x_3 + B_{23}x_2x_3 + B_{123}x_1x_2x_3 \quad (16)$$

Where B_0 is the overall mean, B_1 is an independent effect of the first factor, B_{12} is the first interaction effect, and x_1 is the coded variable. This type of analysis incorporates assumptions that the factors are fixed, the design is completely randomized, and that there exists a normal distribution.

The 2^3 factorial method enabled us to identify the significant factors effecting the slag bath temperature, and utilize the response optimizer to determine the ideal factors to achieve an optimum value of the response.

Once the optimized values for the slag bath were determined, the cost for the auxiliary heating was determined in Appendix E. This cost was calculated by the heat required to raise the slag bath from the reactor temperature to the required bath temperature to maintain fluidity through the tap, coupled with the cost of the heat loss from the bath during normal operation.

CHAPTER 4

RESULTS

4.1 Water Cooling Channels Simulation

The CFD analysis on the water cooling channels was used to determine the energy absorbed by the water that was one of the flux outputs from the reports manager. Regression analysis was then utilized in Microsoft Excel to determine a polynomial function to determine the energy absorbed by the water cooling channels based on the temperature of the liquid slag (Figure 6).

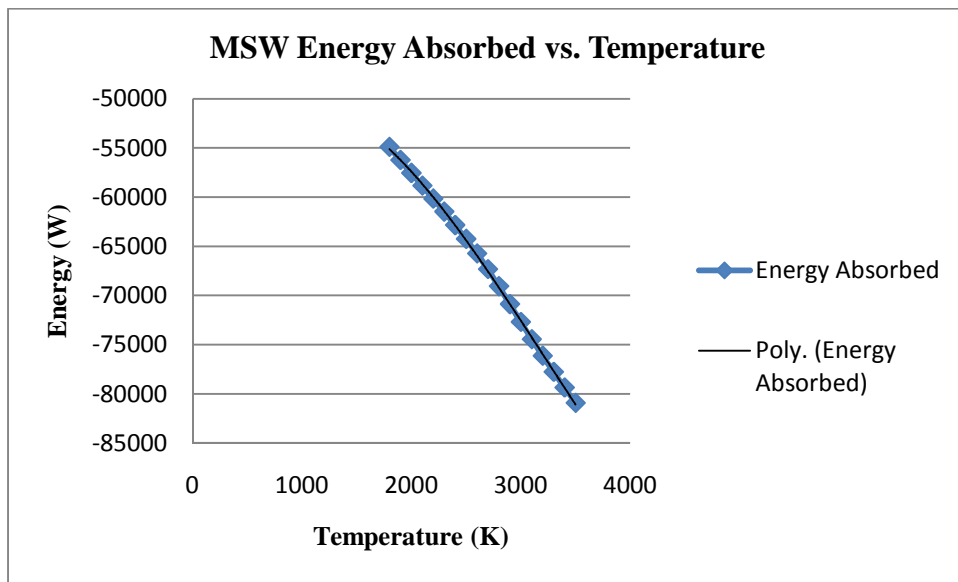
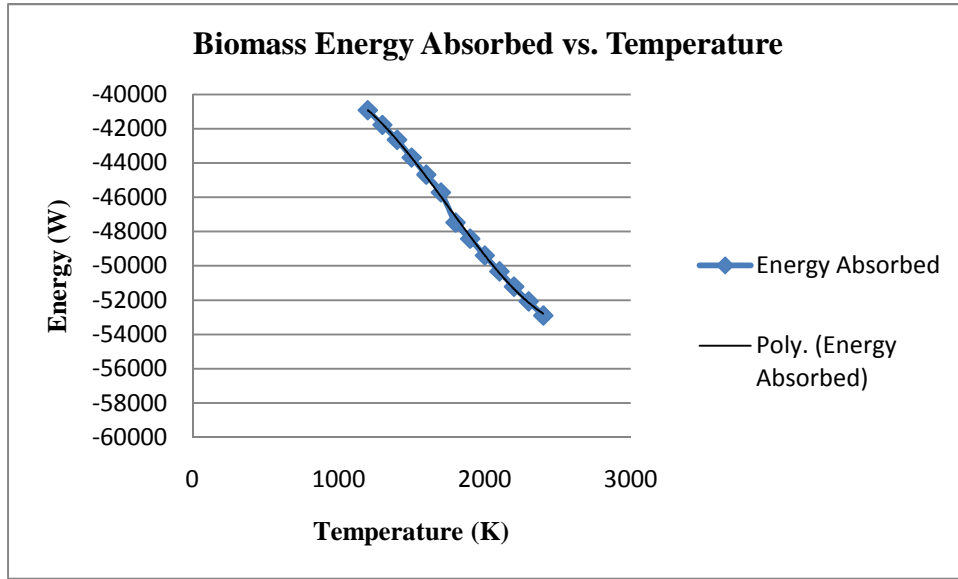


Figure 6. Energy Absorbed by Water Cooling Channels

From these curves the following equation for the energy absorbed by the water cooling channels as a function of temperature for biomass could be expressed as:

$$E = 5e^{-6} * T^3 - 0.0253 * T^2 + 32.675 * T - 51987 \quad (17)$$

The function for coal and MSW was the same, as the dominant oxide in the slag for both coal and MSW was silicone dioxide. The function could be expressed as:

$$E = 1e^{-6} * T^3 - 0.0107 * T^2 + 17.305 * T - 58050 \quad (18)$$

4.2 Specific Heat and Thermal Conductivity

The coefficients from the NIST Chemistry Webbook were used with Equation 1 to determine the specific heat and thermal conductivity for a range of temperatures for each individual oxide. Utilizing this data, regression analysis was conducted in Microsoft Excel that can be seen in Appendix F to determine coefficients needed for the form of Equation 2 (Table 3).

Table 3. Specific Heat and Thermal Conductivity Coefficients for Fluent

Material		SiO2		Al2O3	
Property		Cp (J/mol*K)	K (W/m*K)	Cp (J/mol*K)	K (W/m*K)
Coefficients	1	-1.09E+02	-2.67E+00	-1.11E+01	-1.96E-01
	2	7.56E-01	1.94E-02	4.59E-01	8.10E-03
	3	-1.30E-03	-4.00E-05	-6.00E-04	-1.00E-05
	4	1.00E-06	5.00E-08	5.00E-07	8.00E-09
	5	-4.00E-10	-3.00E-11	-2.00E-10	-3.00E-12
	6	7.00E-14	1.00E-14	2.00E-14	4.00E-16
	7		-1.00E-18		

Material		TiO2		CaO	
Property		Cp (J/mol*K)	K (W/m*K)	Cp (J/mol*K)	K (W/m*K)
Coefficients	1	4.53E+00	1.08E-01	2.59E+01	6.97E-01
	2	2.72E-01	6.50E-03	7.74E-02	2.10E-03
	3	-4.00E-04	-1.00E-05	-9.00E-05	-2.00E-06
	4	3.00E-07	8.00E-09	5.00E-08	1.00E-09
	5	-1.00E-10	-3.00E-12	-1.00E-11	-3.00E-13
	6	2.00E-14	5.00E-16	1.00E-15	3.00E-17

Material		MgO		Na2O	
Property		Cp (J/mol*K)	K (W/m*K)	Cp (J/mol*K)	K (W/m*K)
Coefficients	1	1.58E+01	6.32E-01	3.65E+01	6.02E-01
	2	1.02E-01	4.10E-03	1.47E-01	2.40E-03
	3	-1.00E-04	-5.00E-06	-1.00E-04	-2.00E-06
	4	7.00E-08	3.00E-09	7.00E-08	1.00E-09
	5	-2.00E-11	-7.00E-13	-1.00E-11	-2.00E-13
	6	2.00E-15	8.00E-17		

Table 3.—Continued.

Material		K2O		P2O5	
Property		Cp (J/mol*K)	K (W/m*K)	Cp (J/mol*K)	K (W/m*K)
Coefficients	1	2.27E+01	2.55E-01	4.62E+01	3.50E-01
	2	3.98E-01	4.50E-03	6.35E-01	4.80E-03
	3	-9.00E-04	-1.00E-05	-3.00E-04	-2.00E-06
	4	1.00E-06	1.00E-08	4.00E-08	3.00E-10
	5	-8.00E-10	-9.00E-12		
	6	3.00E-13	3.00E-15		
	7	-4.00E-17	-4.00E-19		

Material		SiO3	
Property		Cp (J/mol*K)	K (W/m*K)
Coefficients	1	1.91E+01	2.07E-01
	2	1.41E-01	1.50E-03
	3	-1.00E-04	-1.00E-06
	4	7.00E-08	7.00E-10
	5	-2.00E-11	-2.00E-13
	6	2.00E-15	2.00E-17

Table 3.—Continued.

Material		Fe ₂ O ₃		
Temp (K)		298-900		
Coefficients	Property	C _p (J/mol*K)	K (W/m*K)	
	1	1.68E+02	3.96E-01	
	2	2.23E+00	5.30E-03	
	3	-2.40E-03	-6.00E-06	
	4	1.00E-06	3.00E-09	
	Temp (K)		900-1050	
	Property	C _p (J/mol*K)	K (W/m*K)	
	1	9.43E+02	2.22E+00	
	Temp (K)		1050-3500	
	Property	C _p (J/mol*K)	K (W/m*K)	
	1	8.27E+02	1.95E+00	
	2	4.32E-02	1.00E-04	
	3	1.00E-05	2.00E-08	
	4	-5.00E-09	-1.00E-11	

The coefficients were all found for a standard polynomial equation, except for iron oxide. This particular oxide had to be analyzed as a piecewise polynomial equation due to the complex characteristics of its curve.

4.3 Viscosity

The results from the calculations for viscosity for coal, biomass, and MSW are in Table 4.

Table 4. Viscosity Groupings and Constants

	Property	Coal	Biomass	MSW
Grouping	x_g	4.95E-01	4.62E-01	5.37E-01
	x_m	1.11E-01	4.85E-01	2.72E-01
	x_a	4.06E-01	5.16E-02	2.05E-01
Constant	α	2.14E-01	9.04E-01	5.70E-01
	b_0	2.03E+01	1.39E+01	2.22E+01
	b_1	1.13E+01	3.08E+01	5.95E+00
	b_2	- 4.55E+00	- 7.45E+01	- 5.04E+00
	b_3	3.75E+01	9.41E+01	4.16E+01
	b	2.94E+01	1.76E+01	3.04E+01
	a	3.13E-10	7.39E-09	2.36E-10

With these constants for the various types of slag, curves for the viscosity of the slag versus temperature could be created (Figure 7). In addition to the theoretical curves generated, an experimental curve (Ilyushechkin et al. 2010) was plotted for the same coal that was analyzed through the defined theoretical process.

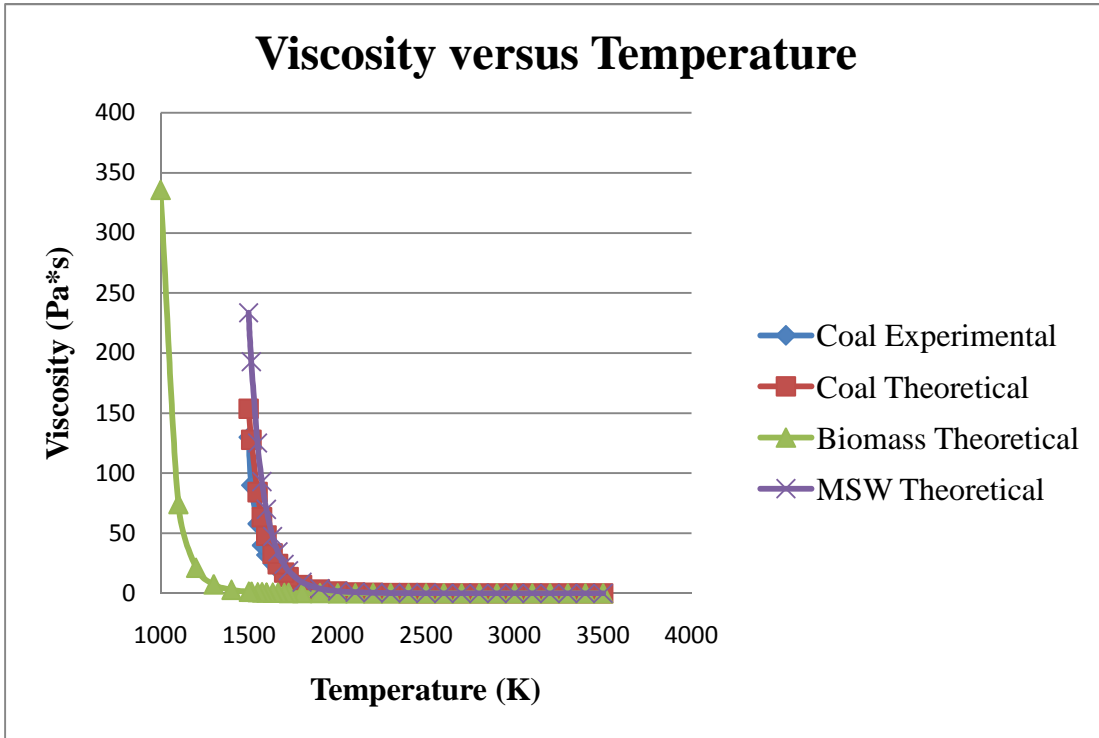


Figure 7. Slag Viscosity versus Temperature

4.4 Model Simulation

The slag tapping model was analyzed for 24 separate cases. There were 8 cases tested for each slag type. Once all of the analyses were complete, the maximum and minimum values for both temperature and viscosity from all of the test cases were recorded. These values were then used to generate a standard set of contour values for each test case for these properties. This was done so that the fluid profiles of the slag from different materials and varying geometry could be compared.

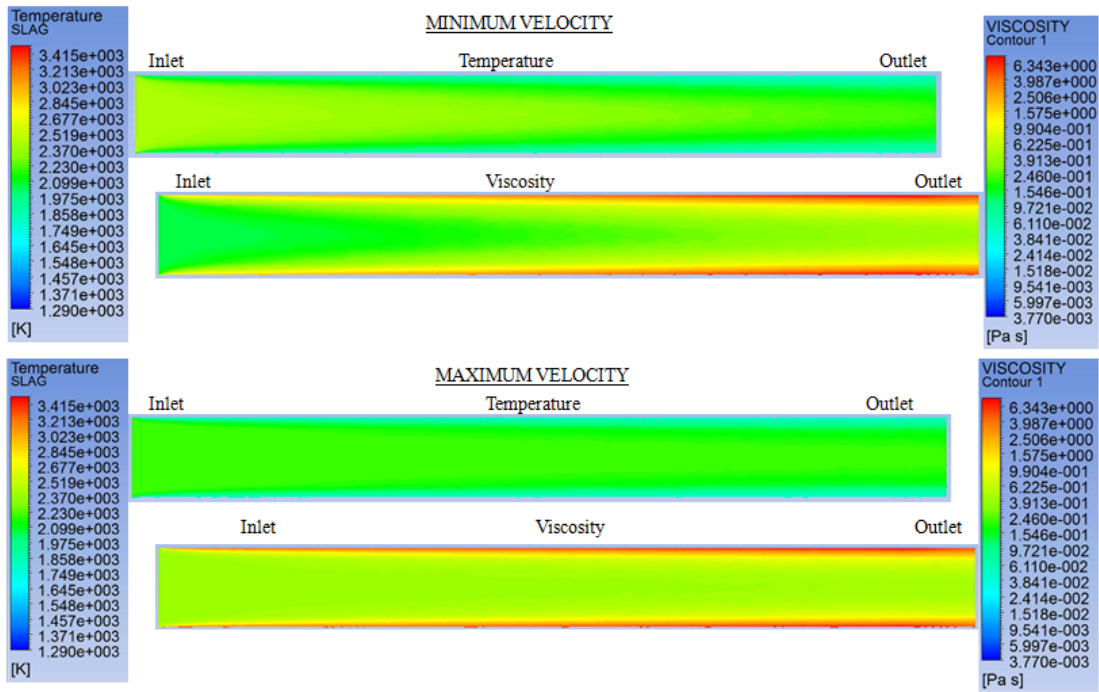


Figure 8. Temperature and Viscosity Contours for Coal Slag for Minimum Diameter and Minimum Length

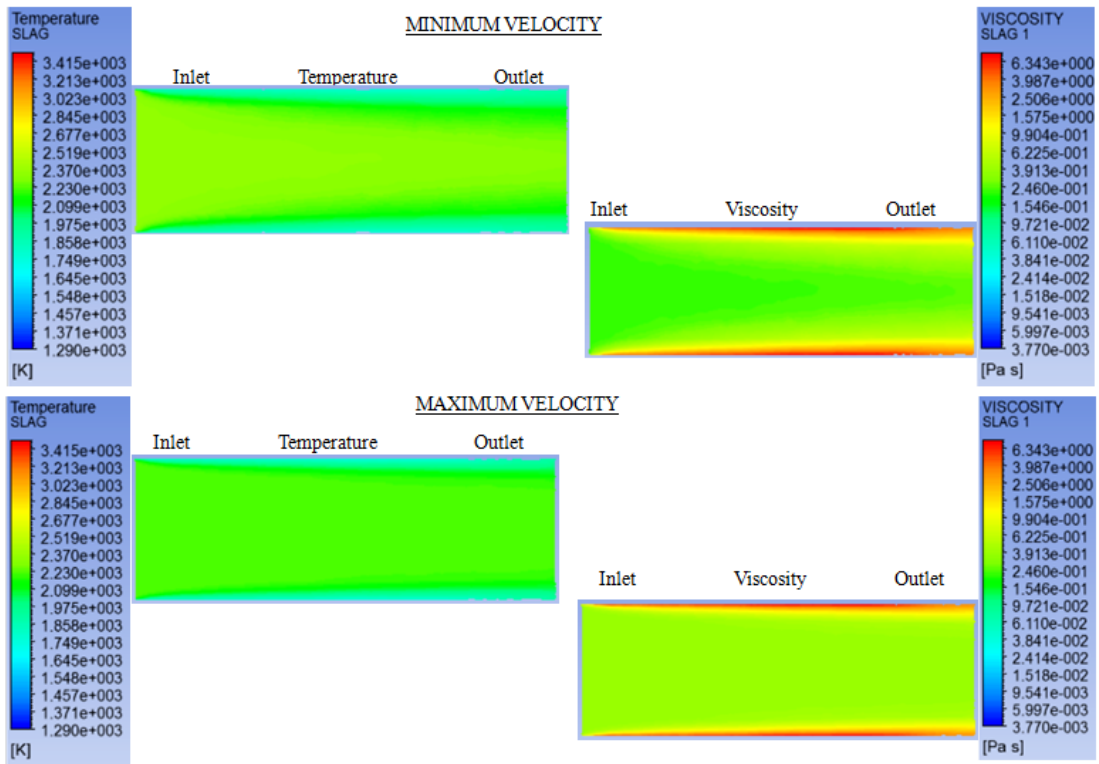


Figure 9. Temperature and Viscosity Contours for Coal Slag for Maximum Diameter and Minimum Length



Figure 10. Temperature and Viscosity Contours for Coal Slag for Minimum Diameter and Maximum Length

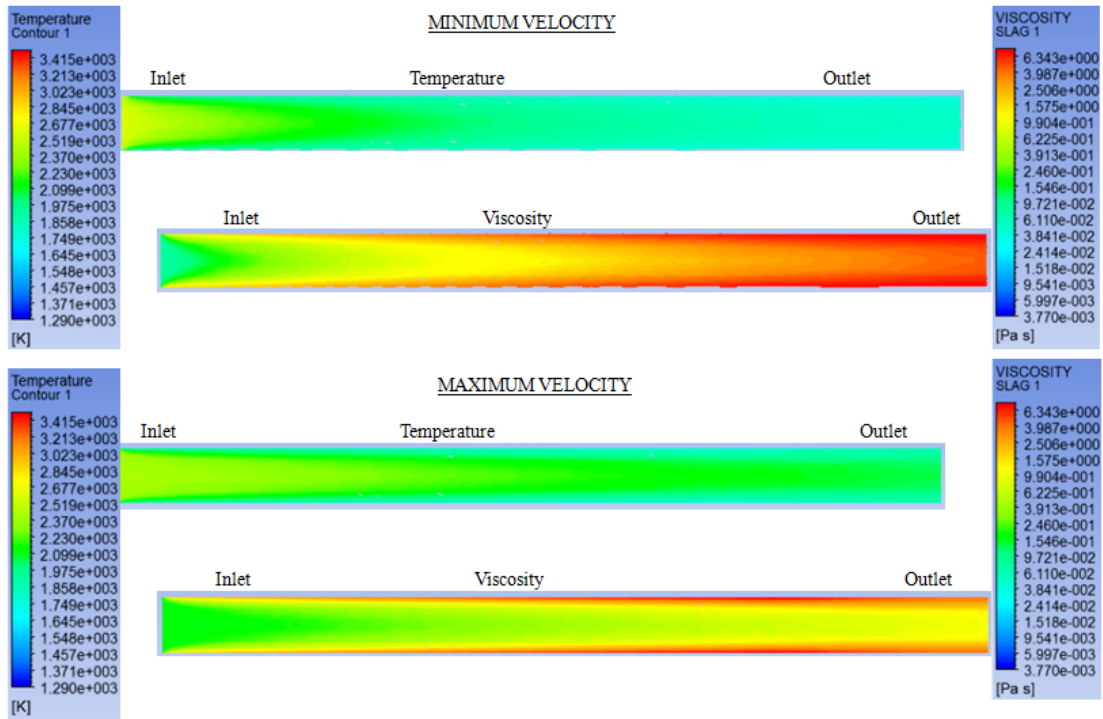


Figure 11. Temperature and Viscosity Contours for Coal Slag for Maximum Diameter and Maximum Length

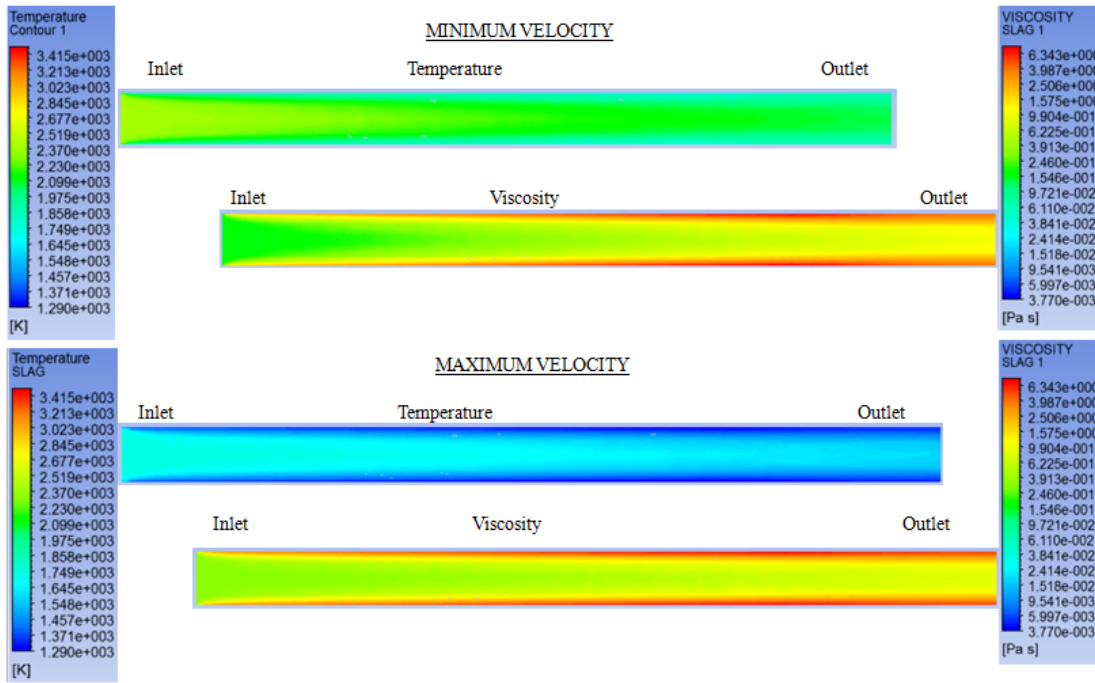


Figure 12. Temperature and Viscosity Contours for Biomass Slag for Minimum Diameter and Minimum Length

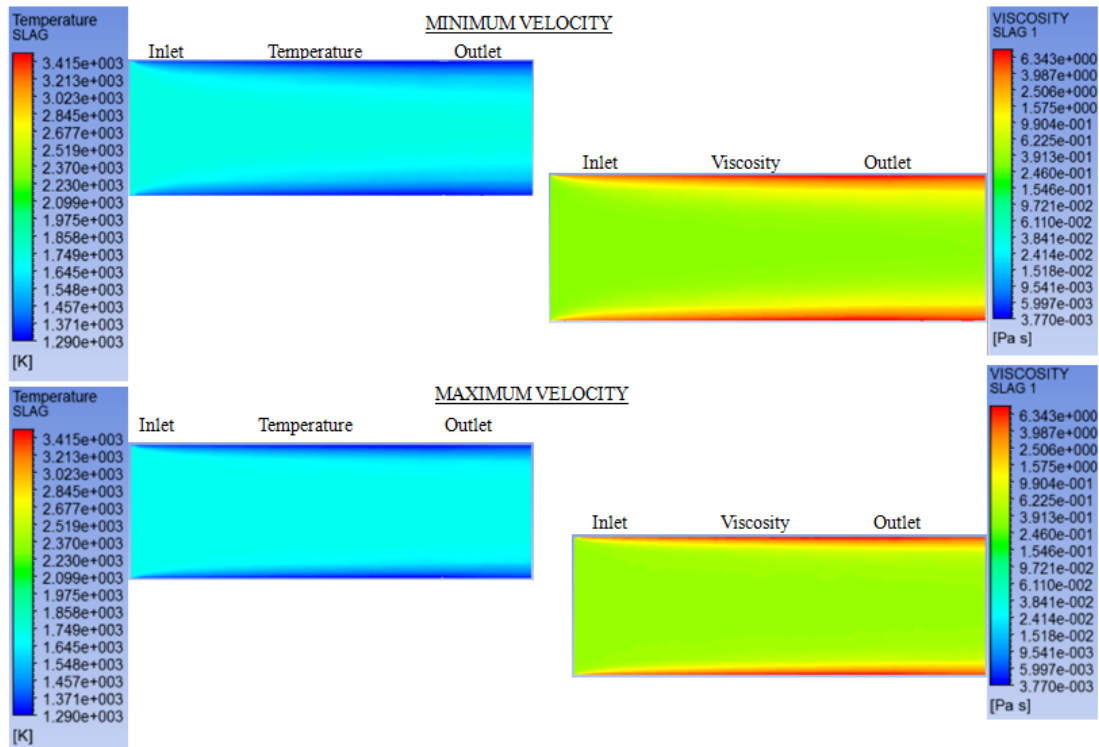


Figure 13. Temperature and Viscosity Contours for Biomass Slag for Maximum Diameter and Minimum Length

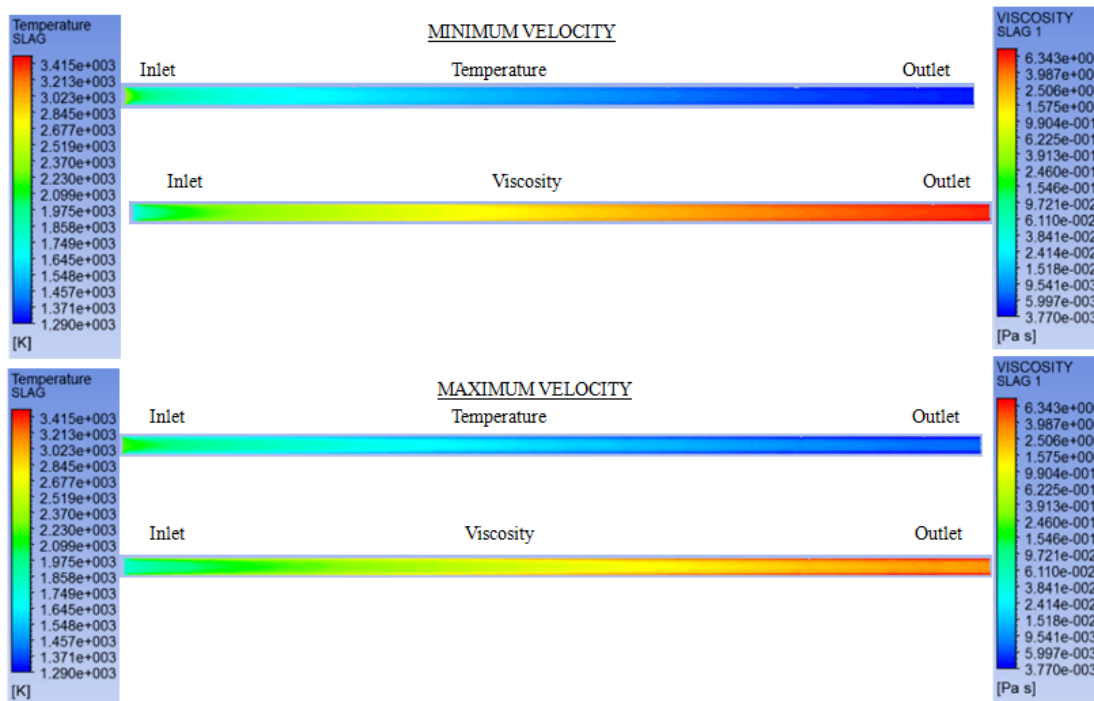


Figure 14. Temperature and Viscosity Contours for Biomass Slag for Minimum Diameter and Maximum Length

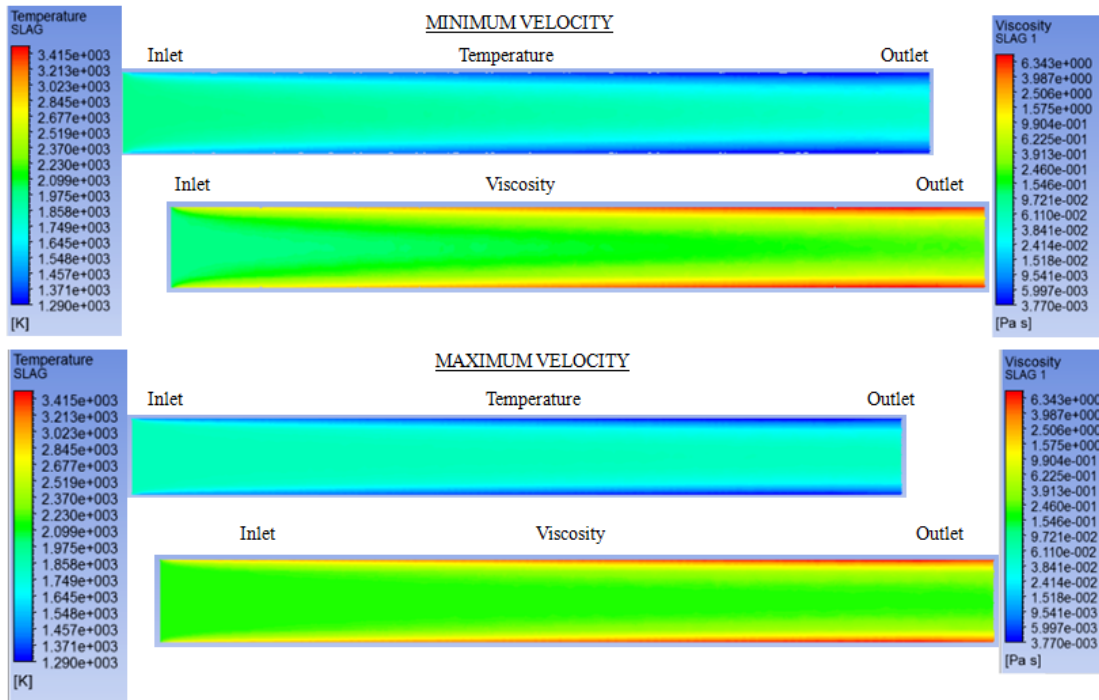


Figure 15. Temperature and Viscosity Contours for Biomass Slag for Maximum Diameter and Maximum Length

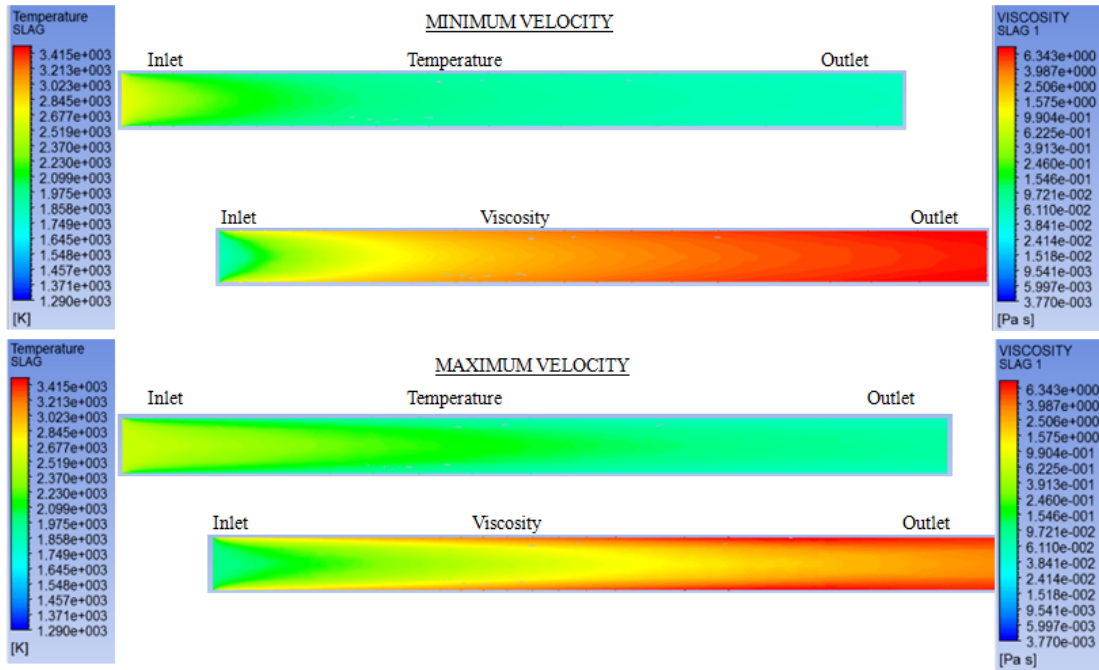


Figure 16. Temperature and Viscosity Contours for MSW Slag for Minimum Diameter and Minimum Length

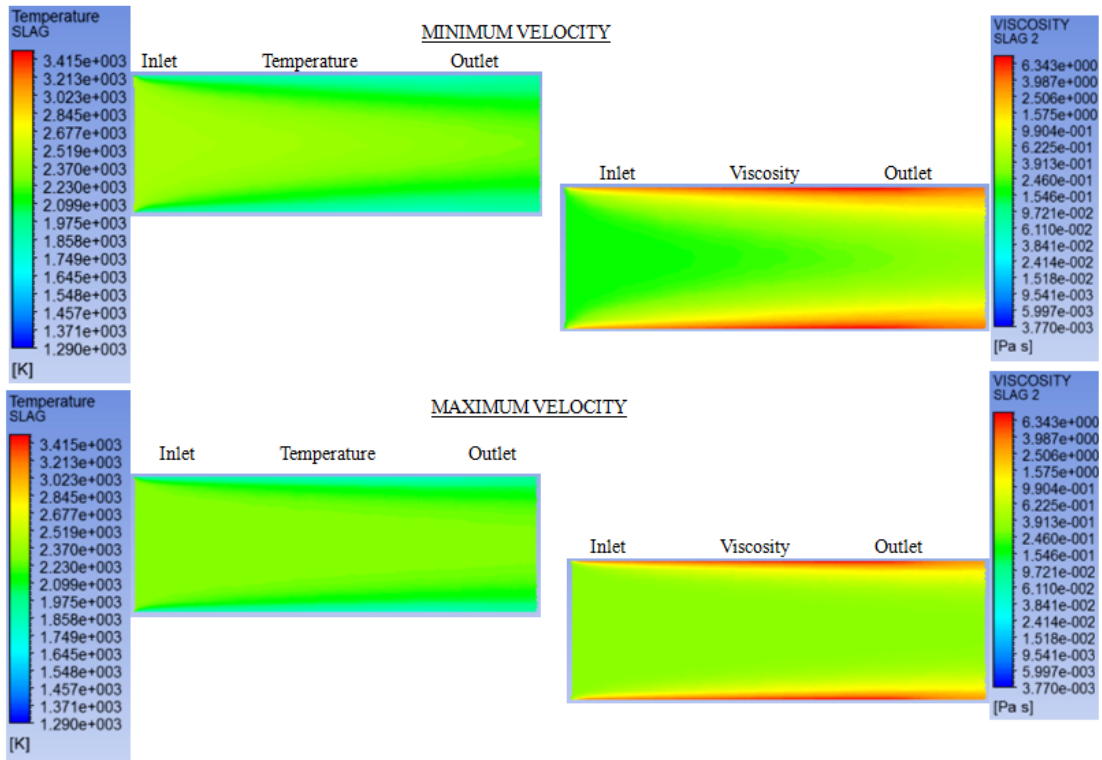


Figure 17. Temperature and Viscosity Contours for MSW Slag for Maximum Diameter and Minimum Length

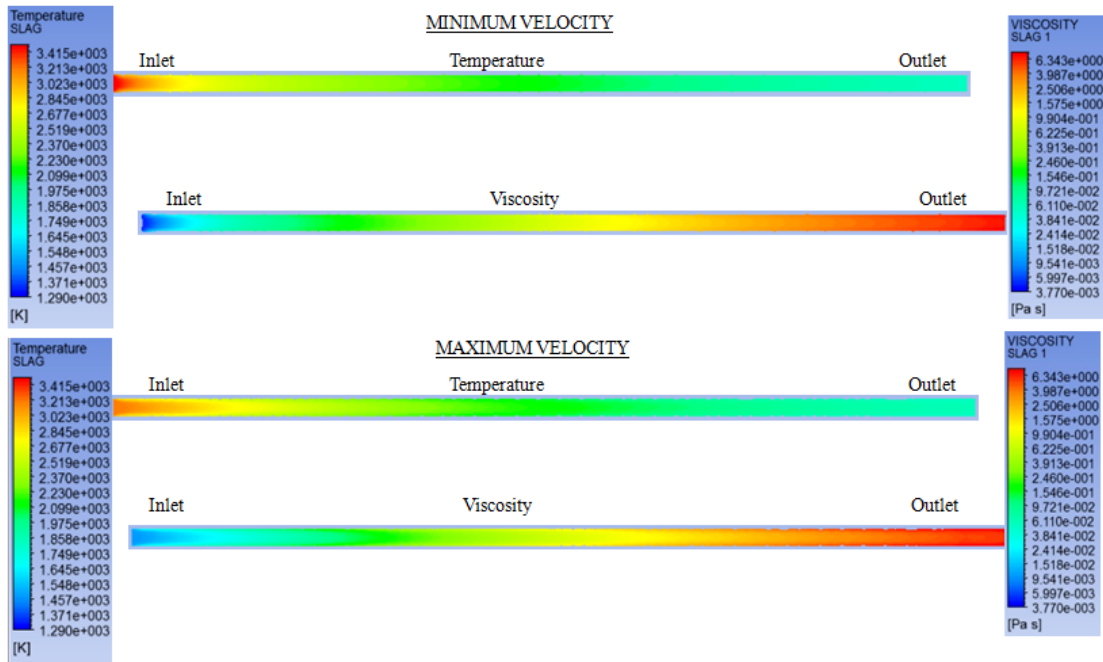


Figure 18. Temperature and Viscosity Contours for MSW Slag for Minimum Diameter and Maximum Length

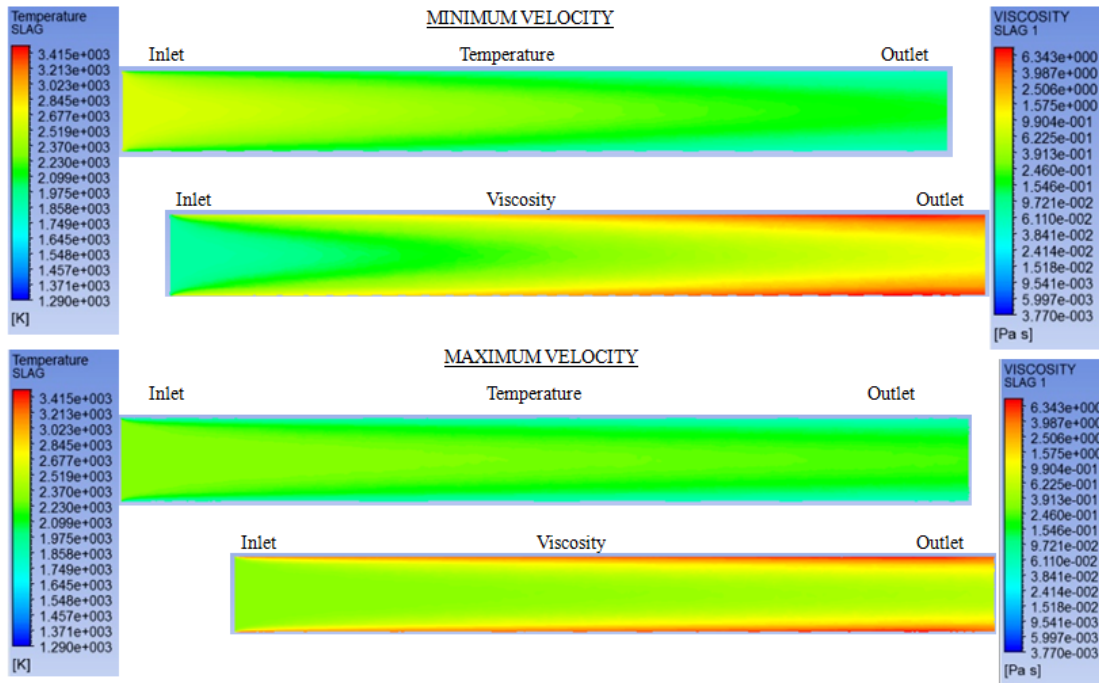


Figure 19. Temperature and Viscosity Contours for MSW Slag for Maximum Diameter and Maximum Length

4.5 Design of Experiments

Each slag material was analyzed individually with a DOE 2^3 full factorial design method. The data being analyzed in the factorial design analysis can be seen in Table 5.

Table 5. Factorial Design Data

Biomass							
Std Order	Run Order	CenterPt	Blocks	Diameter (in)	Length (in)	Velocity (in/s ²)	Biomass Slag Bath Temperature (K)
1	4	1	1	0.5	6	2.97	1787.488
5	1	1	1	0.5	6	11.89	1743.293
3	8	1	1	0.5	24	2.97	2195.087
7	6	1	1	0.5	24	11.89	2079.505
2	5	1	1	2.5	6	2.97	1701.118
6	3	1	1	2.5	6	11.89	1682.341
4	7	1	1	2.5	24	2.97	1927.963
8	2	1	1	2.5	24	11.89	1818.714

Table 5. –Continued.

MSW							
Std Order	Run Order	CenterPt	Blocks	Diameter (in)	Length (in)	Velocity (in/s ²)	MSW Slag Bath Temperature (K)
1	4	1	1	0.5	6	2.97	2638.56
5	8	1	1	0.5	6	11.89	2506.24
3	7	1	1	0.5	24	2.97	3517.92
7	6	1	1	0.5	24	11.89	3206.25
2	5	1	1	2.5	6	2.97	2394.83
6	2	1	1	2.5	6	11.89	2284.23
4	1	1	1	2.5	24	2.97	2576.84
8	3	1	1	2.5	24	11.89	2279.69

Coal							
Std Order	Run Order	CenterPt	Blocks	Diameter (in)	Length (in)	Velocity (in/s ²)	Coal Slag Bath Temperature (K)
1	1	1	1	0.5	6	2.97	2521.63
5	3	1	1	0.5	6	11.89	2393.64
3	7	1	1	0.5	24	2.97	3375.81
7	6	1	1	0.5	24	11.89	2995.99
2	5	1	1	2.5	6	2.97	2326.79
6	8	1	1	2.5	6	11.89	2226.24
4	4	1	1	2.5	24	2.97	2424.87
8	2	1	1	2.5	24	11.89	2207.33

For each material an initial analysis was conducted where all factors and interactions were analyzed and documented in Appendix D. The main effects plots (Figure 20), cube plots between factors (Figure 21), and interaction plots (Figure 22) display the pertinent information from this first analysis.

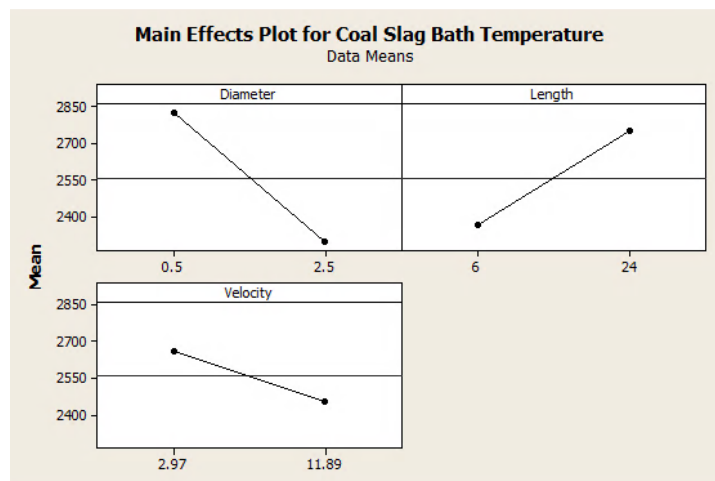
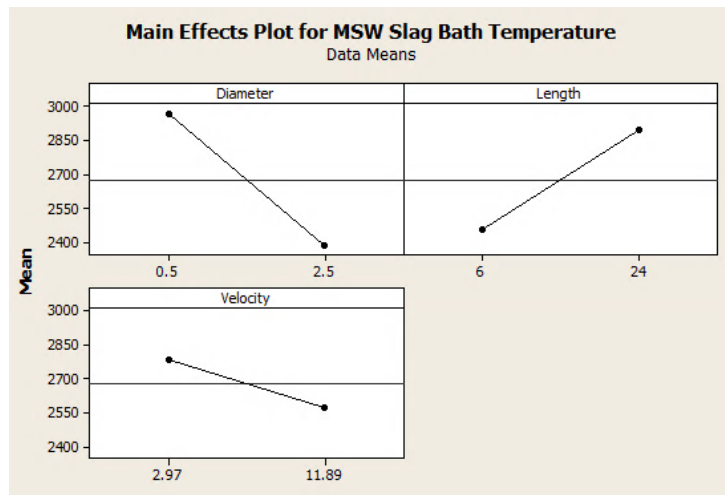
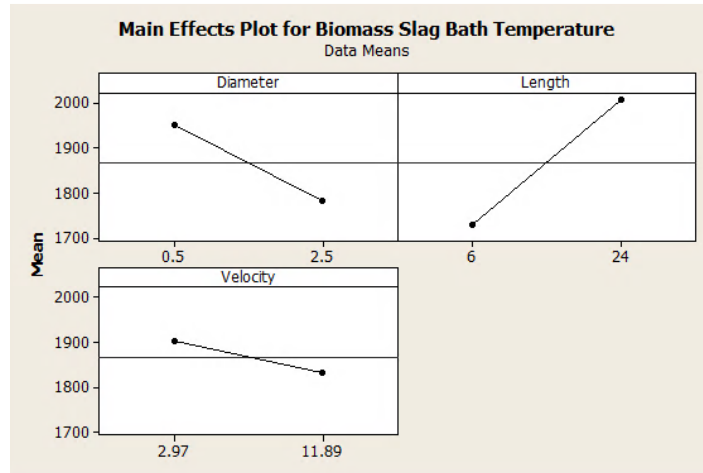


Figure 20. Main Effects Plots for Slag Bath Temperatures

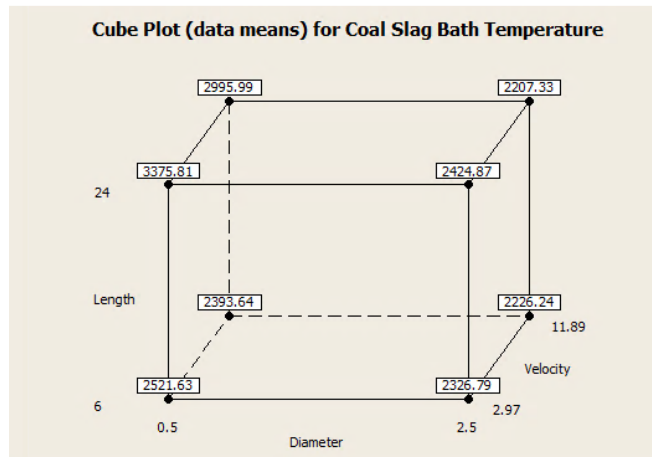
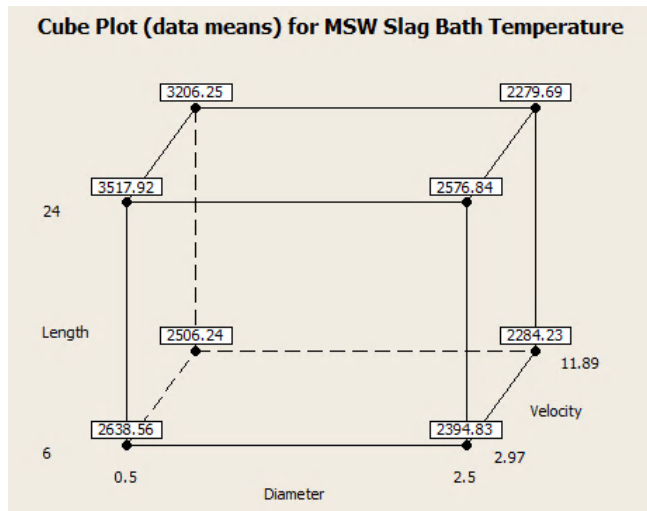
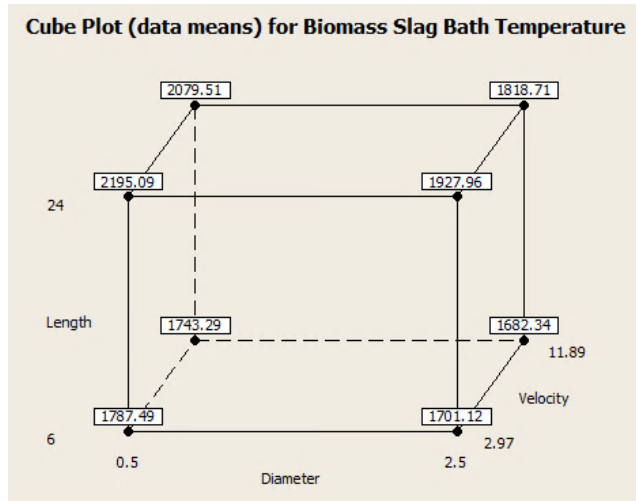


Figure 21. Cube Plot for Slag Bath Temperatures

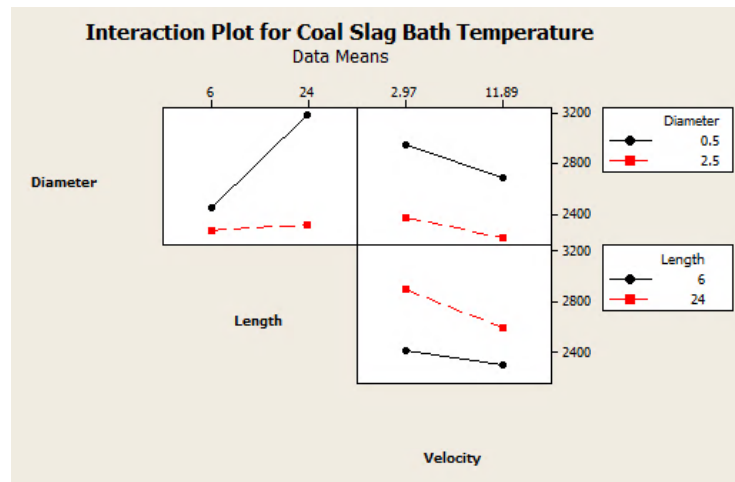
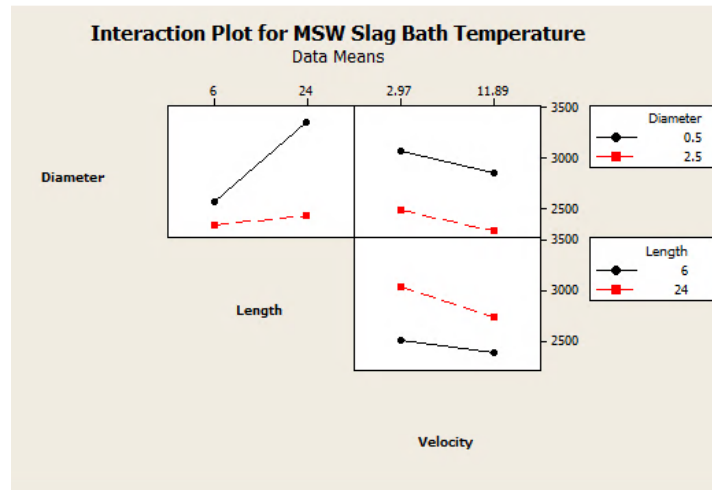
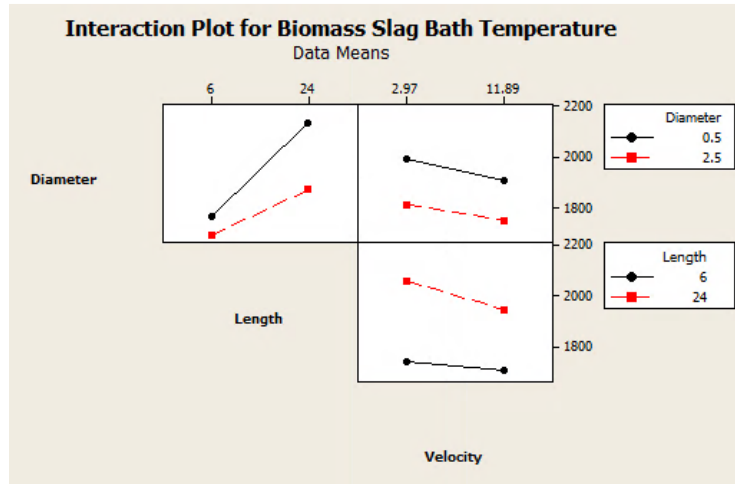


Figure 22. Interaction Plots for Slag Bath Temperatures

The effects results in Appendix D were then analyzed for each material, and effects that were found to not be significant, based on their respective order of magnitude, were removed from the factorial design one at a time. After each term was removed, the 2^3 factorial design was then re-analyzed, and if all of the P-values were less than the assumed alpha of 0.05, the analysis was considered complete. If it was found that there still remained a factor with a P-value higher than 0.05, that factor was removed and the 2^3 factorial design was re-analyzed. The only instance where this was not the procedure, was if the removal of a term significantly reduced the R squared adjusted value, if this occurred then the analysis would be considered complete at this juncture. Once this process was complete for each material, the final analysis output was documented in Appendix D and Pareto charts for the Standardized Effects (Figure 23) were plotted to observe significance of the remaining factors.

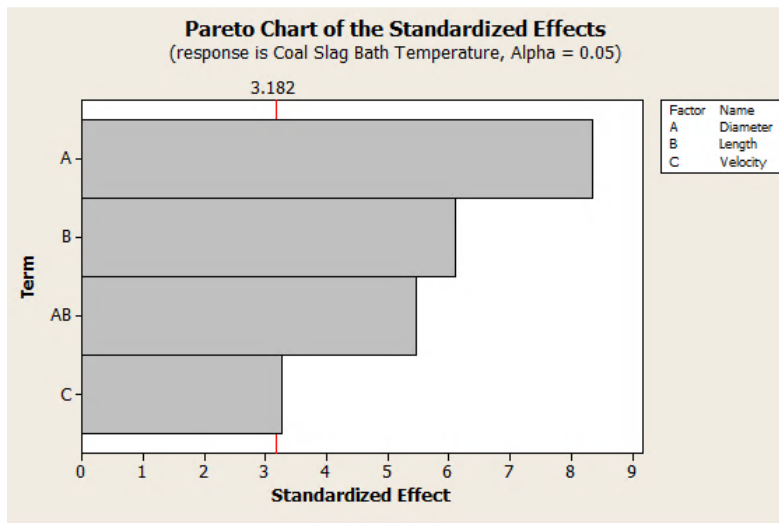
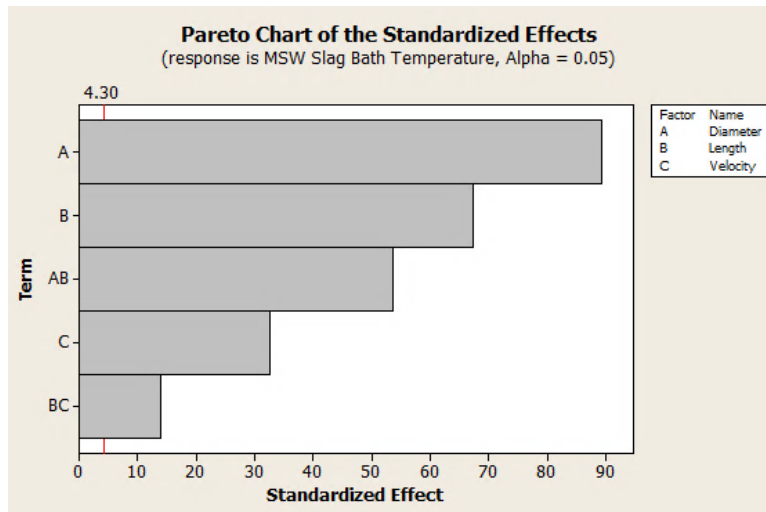
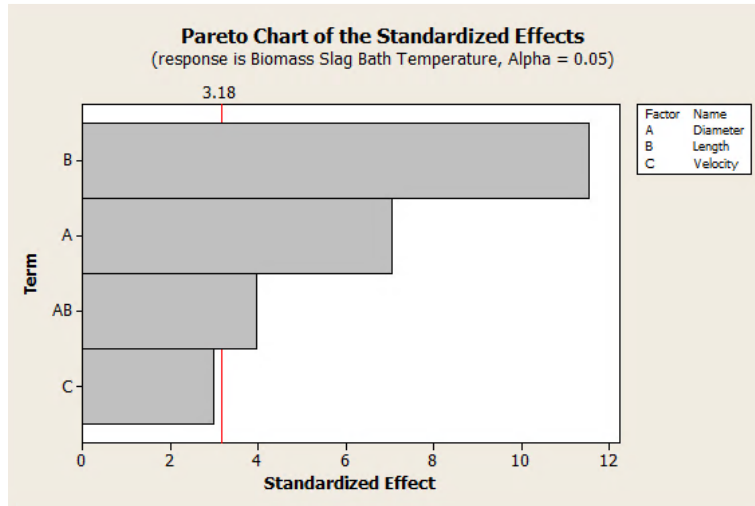


Figure 23. Pareto Charts for the Standardized Effects

The assumptions of the samples being normally distributed and constant variance were checked with normal probability plots (Figure 24) and versus fits (Figure 25) displaying that these assumptions were met.

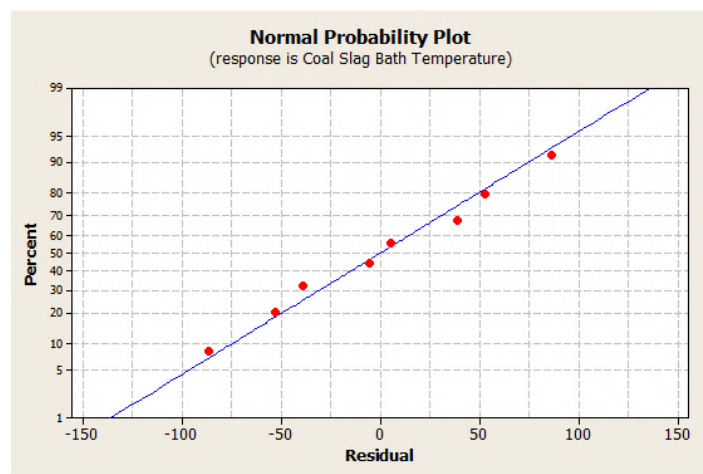
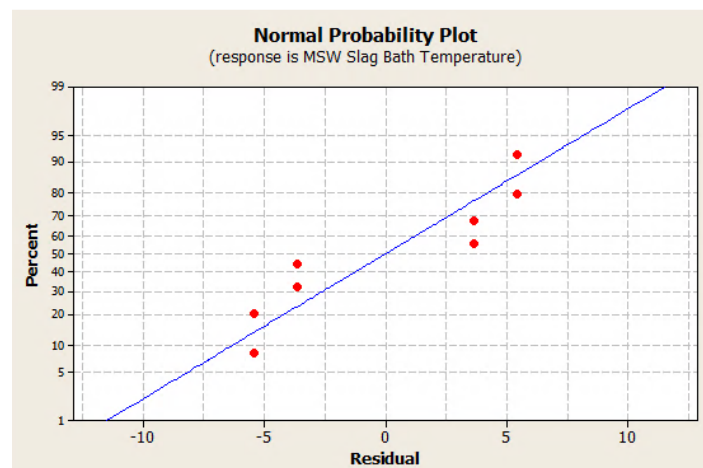
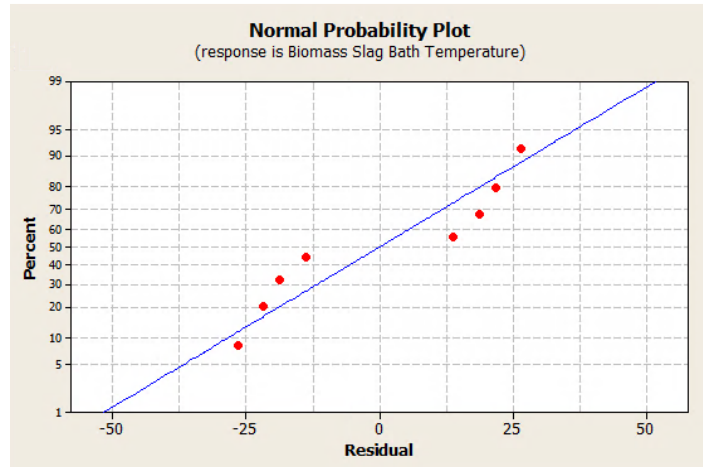


Figure 24. Normal Probability Plots for Slag Bath Temperatures

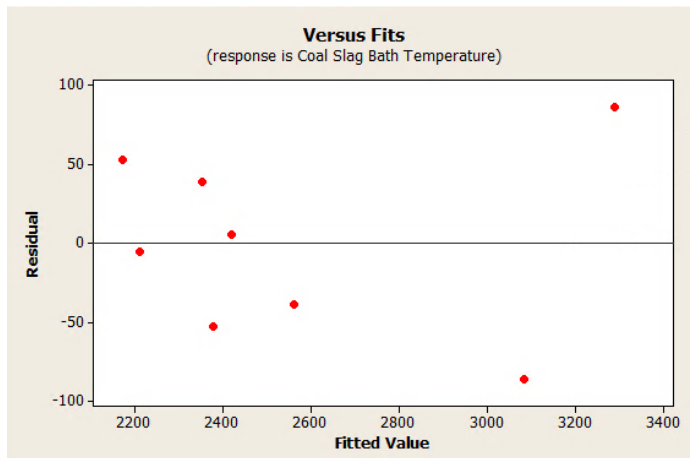
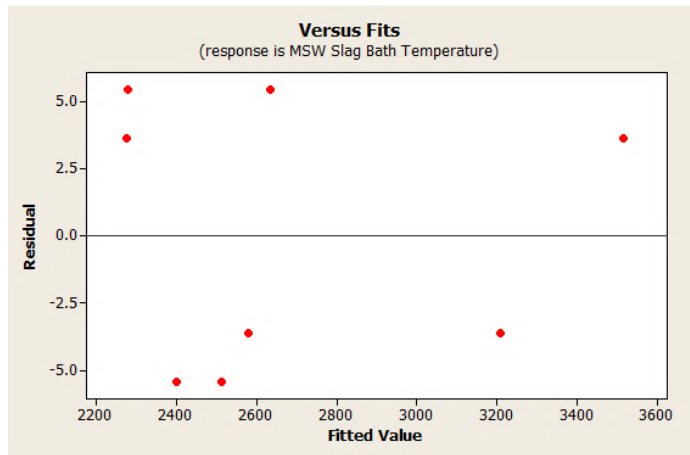
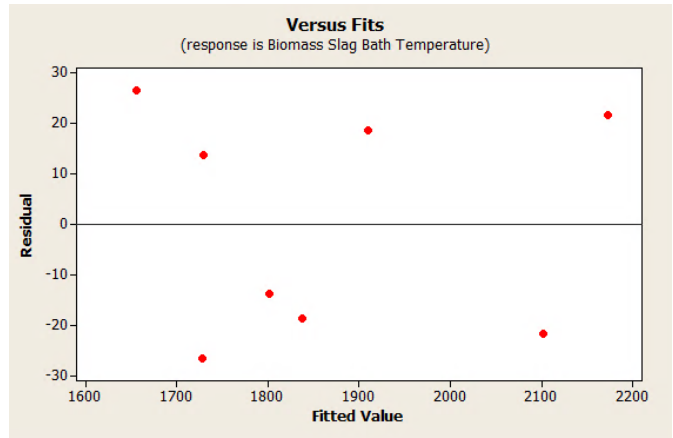


Figure 25. Versus Fits for Slag Bath Temperatures

The linear regression function determined with the statistical analysis for biomass was found to be

$$T = 1866.94 - 84.4Diameter + 138.38Length - 47.57Diameter * Length \quad (19)$$

The model for MSW can be expressed as:

$$T = 2675.6 - 291.7Diameter + 219.6Length - 106.5Velocity - 175.2Diameter * Length - 45.7Length * Velocity \quad (20)$$

The model for coal can be expressed as:

$$T = 2559.0 - 262.7Diameter + 192.0Length - 103.2Velocity - 172.2Diameter * Length \quad (21)$$

The last output from the statistical analysis was from the factorial design response optimizer (Figure 26). This figure displays the combination of input factors that jointly optimize the slag bath temperature response.

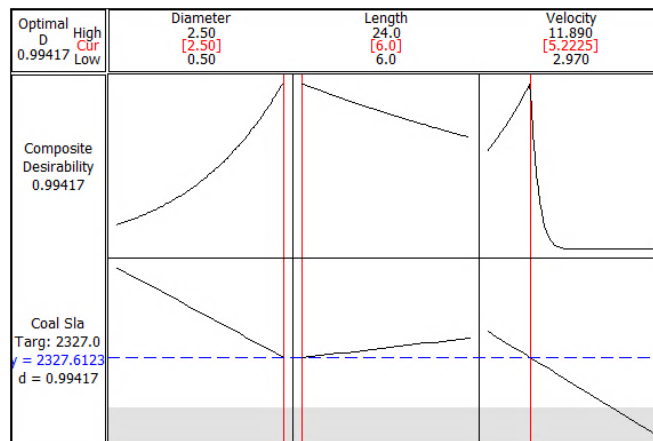
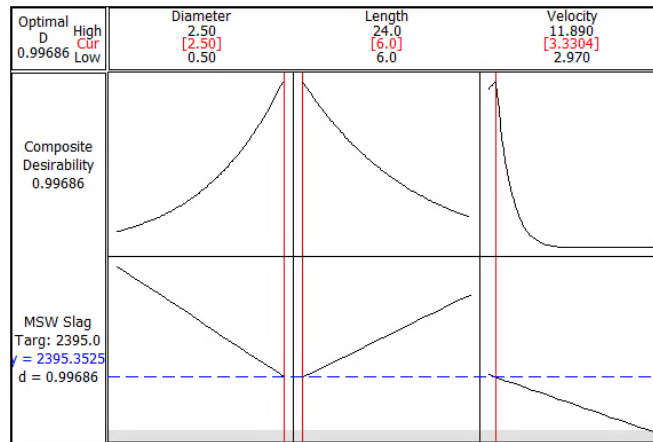
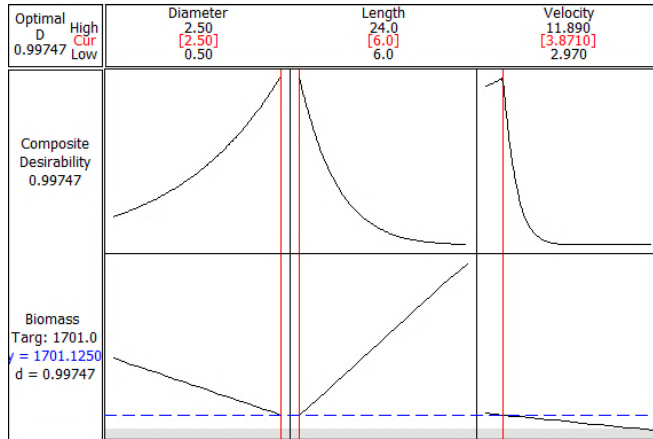


Figure 26. Response Optimizer for Slag Bath Temperature

CHAPTER 5

DISCUSSION

5.1 Model Simulation

The simulation of the slag tapping block in CFD yielded significant results that were validated by the experimental results (Ilyushechkin 2010) for the viscosity of coal slag in a given temperature range in Figure 7. The theoretical results produced in this study followed the same curve as the experimental results, with differences in viscosity within an order of magnitude, which was normal for Urbain's method (Vargas et al. 2000).

The other significant information displayed in Figure 7 was that the lower limit of 8 Pa*s for viscosity was properly chosen. It was observed that after 10 Pa*s the slag viscosity began to increase rapidly which was a sign that the slag diverged from behaving as a Newtonian Fluid and became Non-Newtonian. The temperature of critical viscosity was in this region, and when the temperature of the slag reaches this point the composition of the slag is changed from a one phase to a two or more phase mixture (Vargas et al. 2000). This would have affected the analysis being conducted in CFD as the assumption for the analysis was that the slag was a one phase liquid mixture.

The model simulation also provided valuable data on how the profile of the fluid in the slag tapping channel would behave during discharge from the slag bath. These profiles were valuable for comparing how the same type of slag reacted with

varying velocities and geometries, but also as a means to compare how the different types of slag compared to each other.

Observing Figure 11, for the 2.5 inch diameter by 24 inch length channel with coal slag, it was discerned that the area where the viscosity was reaching the limit of $8 \text{ Pa}\cdot\text{s}$ was dominant in the outlet region for the slag at the low velocity. However, for the high velocity, this increased viscosity was only prevalent around the fluid edges where it was interfacing with the pipe. Comparing Figure 11 with Figure 9, for the 2.5 inch diameter and 6 inch length channel for coal slag, the difference in the viscosity profiles between the high and low velocity was almost negligible.

Comparing the coal slag from Figure 9 with the biomass slag in Figure 13, it was observed that the maximum fluid temperature of the biomass slag was under 2000 K, whereas the coal slag was in the range of 2500 K. The temperature profile of the MSW slag in Figure 17, for the 2.5 inch diameter and 6 inch channel length, was much closer to the range for the coal slag. This was likely due to the higher concentrations of silicon dioxide in both coal and MSW slag (Table 1) in comparison to biomass slag. This was in part due to pure silica having a very high viscosity and melt temperature compared to the other oxides comprising the slag.

The CFD analysis also verified some of the intuitive assumptions about the factors affecting the slag tapping block. The CFD analysis showed how the treatment consisting of maximum diameter, minimum length, and maximum velocity resulted in the ideal response in the slag bath temperature for all of the slag materials. This observation intuitively made sense and was observed in the cube plots for each material in Figure 21. However, it was not possible to determine from the CFD

analysis how much each factor affected this response, nor the effect of the interaction of the factors.

The statistical analysis results provided the means to quantitatively represent how the factors of diameter, length, velocity, and the associated interactions affected the response of the slag bath temperature. They also provided a means to optimize the response through the ideal utilization of the factors. The results of the 2^3 factorial design provided main effect values for each individual factor as well as the interactions for each slag type (Appendix D).

The individual factor with the strongest effect for the biomass slag was the length of the tapping channel. This was observed visually in the main effects plot in Figure 20, where the length factor clearly had the steepest slope. The most significant interaction was between the diameter and length factors seen in the interaction plot in Figure 22. It was also observed in this interaction plot that the lines for diameter and velocity were almost parallel, signifying a minimal effect from the interaction of the diameter and velocity factors.

Similar to biomass, the interaction with the strongest effect for both MSW and coal was found to be from the diameter and length factors. Based on the main effect values (Appendix D) and interaction plots (Figure 22) for biomass, MSW, and coal, this interaction had an even stronger effect on the response than the individual velocity factor. MSW and coal results differed from biomass in the individual factor that had the strongest effect. For both MSW and coal, the diameter had the most significant effect, whereas for biomass the length was the most significant. This discrepancy in individual factor effects may have been due to the much higher

temperatures for the slag bath required for both MSW and coal in comparison to the lower temperature ranges for biomass. This difference was also reflected in the CFD output in Table 5, where for both MSW and coal the length had very little effect on the slag bath temperature when the diameter was set at the maximum value.

Based on the statistical analysis results for the 2^3 factorial design for the varying types of slag, it was determined that the maximum diameter and minimum length for the slag tapping channel should be incorporated for the optimized design. As the feedstock for gasification may vary at a particular plant, the slag tap should be optimized for a range of slag types. The factorial design results for coal and MSW clearly depicted that the diameter and length had the strongest individual and interaction effects. Although velocity had a significant effect for these slag types, it was minimal in comparison with length and diameter, and for biomass the velocity was not even significant based on the P-value. In optimizing the design of the slag tapping channel for all of these material types velocity will not be considered significant and the minimum velocity will be used for the slag bath temperature. In addition to the lower effect values for the velocity, the other reason to minimize this factor is that in order to raise the velocity of the slag a larger slag bath would need to be constructed which would require an increased capital cost and increased auxiliary heating of the slag bath.

The factorial design response optimizer was then utilized to assist in justifying the decision to not include velocity as a significant factor. The results in Figure 26 display how the input variable of velocity was maintained at a lower value for all slag

types, while the diameter was maximized and the length was minimized to create the targeted slag bath temperature that was the desired response.

The optimized slag bath temperature for biomass was found to be 1701 K, for MSW to be 2394 K, and for coal to be 2327 K (Table 5). The optimized temperature was based on the design that would result in the minimum allowable slag bath temperature based on significant factors that would result in fluidized slag throughout the tapping channel. The auxiliary heating cost for the biomass was found to be approximately \$79,400, which was significantly less than the cost for MSW \$108,400, and coal \$105,600. However, the additional cost savings that results from not having to send MSW to a landfill should also be considered. Appendix E also shows how the design without optimization resulted in significantly larger auxiliary heating costs. The auxiliary heating costs increased to \$99,100 for biomass, \$153,700 for MSW, and \$147,800 for coal.

5.2 Future Work

Moving forward, the model could be improved by adding center points to the 2³ factorial design method. The addition of center points could serve to check the assumption of linearity in the factor effect and construct an estimate of error for the factorial design when all degrees of freedom are consumed from the full set of interactions.

The CFD model for defining the material properties of the slag based on Urbain's method and data from NIST could also be written entirely in C++ code and interpreted into CFD as a compiled library. This could then be incorporated into a more complete gasification model, similar to what Wang and Silaen (Wang and

Silaen 2007) conducted where combustion of feedstocks was modeled in addition to heat transfer and particle tracking in the gasification region.

5.3 Conclusions

This model for slag flow from sustainable feedstocks has been corroborated based on comparisons with baseline coal experimental results for slag viscosity. The model of the slag tapping channel successfully produced tangible results for determining the auxiliary heating required for the slag bath. Through relating the temperature differential for the gasification reactor temperature to the required slag bath temperature for biomass, MSW, and coal slag, a cost for the auxiliary heating cost of the slag bath was determined. This model also revealed the significance of factors affecting the geometry and flow of the fluid slag and how best to optimize the slag tapping channel.

Appendix A

Interpreted Viscosity Equation for Fluent

```
#include "udf.h"
```

```
DEFINE_PROPERTY(cell_viscosity, c, t)
```

```
{
```

```
real mu_lam;
```

```
real temp = C_T(c, t);
```

```
mu_lam = 3.12902e-10*temp*exp(29372.55858/temp);
```

```
return mu_lam;
```

```
}
```

```
#include "udf.h"
```

```
DEFINE_PROPERTY(cell_viscosity, c, t)
```

```
{
```

```
real mu_lam;
```

```
real temp = C_T(c, t);
```

```
mu_lam = 7.38879e-9*temp*exp(17631.64363/temp);
```

```
return mu_lam;
```

```
}
```

```
#include "udf.h"
```

```
DEFINE_PROPERTY(cell_viscosity, c, t)
```

```
{
```

```
  real mu_lam;
```

```
  real temp = C_T(c, t);
```

```
  mu_lam = 2.35777e-10*temp*exp(30.423.45425/temp);
```

```
  return mu_lam;
```

```
}
```

Appendix B

Heat Transfer Coefficient for Copper Pipe

The heat transfer coefficient for convection for the pipe was found assuming the fluid in contact with the pipe at the outlet would be at the minimum temperature for each slag material type. So the temperature of the slag for biomass was approximated as 1292°K, the temperature for MSW was 1818 °K, and the temperature for coal was 1783 °K.

From Table A.4 (Incorpera and DeWitt 2001), the properties of air at atmospheric pressure and the following defined properties could be created:

$$T_{film} = \frac{T_s + T_\infty}{2} \quad (1)$$

$$\beta = 1/T_f \quad (2)$$

Table 1. Properties for Air at Film Temperature

Temperature	Film Temperature	k (W/m*K)	v (m ² /s)	Pr
1818	1059	6.95E-02	1.34E-04	7.27E-01
1783	1041.5	6.87E-02	1.30E-04	7.27E-01
1292	796	5.71E-02	8.42E-05	7.08E-01

Temperature	B	Ra	Nu	h (W/m ² *K)
1818	9.44E-04	9.38E+03	1.49E+01	4.08E+01
1783	9.60E-04	9.82E+03	1.51E+01	4.08E+01
1292	1.26E-03	2.00E+04	1.84E+01	4.14E+01

The values for the Rayleigh number in Table 1 were found from the function expressed as:

$$Ra = \frac{g\beta(T_s - T_\infty)D^3}{\nu^2} Pr \quad (3)$$

The Nusselt number was found from the equation:

$$Nu = \left(0.6 \frac{0.387 * Ra^{\frac{1}{6}}}{\left(1 + \left(\frac{0.559}{Pr} \right)^{\frac{9}{16}} \right)^{\frac{8}{27}}} \right)^2 \quad (4)$$

Finally the heat transfer coefficient was found from the function:

$$h = \frac{k}{d} * Nu \quad (5)$$

Appendix C

Heat Transfer Coefficient for Steel Wall

The heat transfer coefficient for convection for the steel wall was found assuming the steel wall would be at a similar temperature to the copper pipe and block it is contact with.

From Table A.4 (Incorpera and DeWitt 2001), the properties of air at atmospheric pressure and the following defined properties could be created:

$$T_{film} = \frac{T_s + T_\infty}{2} \quad (1)$$

$$\beta = 1/T_f \quad (2)$$

Table 1. Properties for Air at Film Temperature

Temperature	Film Temperature	k (W/m*K)	v (m ² /s)	Pr
1818	1059	6.95E-02	1.34E-04	7.27E-01
1783	1041.5	6.87E-02	1.30E-04	7.27E-01
1292	796	5.71E-02	8.42E-05	7.08E-01
Temperature	B	Alpha	Ra	h (W/m ² *K)
1818	9.44E-04	1.84E-04	1.62E+07	7.62E+00
1783	9.60E-04	1.79E-04	1.70E+07	7.61E+00
1292	1.26E-03	1.20E-04	3.42E+07	7.50E+00

The values for the Rayleigh number in Table 1 were found from the function expressed as:

$$Ra = \frac{g\beta(T_s - T_\infty)L^3}{\nu\alpha} \quad (3)$$

Then the heat transfer coefficient was found from the function:

$$h = \frac{k}{L} \left(0.68 + \frac{0.670Ra^{\frac{1}{4}}}{\left(\left(1 + \left(\frac{0.492}{Pr} \right)^{\frac{9}{16}} \right)^{\frac{4}{9}} \right)} \right) \quad (4)$$

Appendix D

2³ Factorial Design Output

Factorial Fit: Biomass Slag Bat versus Diameter, Length, Velocity

Estimated Effects and Coefficients for Biomass Slag Bath Temperature (coded units)

Term	Effect	Coef
Constant		1866.94
Diameter	-168.81	-84.40
Length	276.76	138.38
Velocity	-71.95	-35.98
Diameter*Length	-95.15	-47.57
Diameter*Velocity	7.94	3.97
Length*Velocity	-40.46	-20.23
Diameter*Length*Velocity	-4.77	-2.39

Analysis of Variance for Biomass Slag Bath Temperature (coded units)

Source	DF	Seq SS	Adj SS	Adj MS	F	P
Main Effects	3	220536	220536	73512	*	*
Diameter	1	56993	56993	56993	*	*
Length	1	153189	153189	153189	*	*
Velocity	1	10354	10354	10354	*	*
2-Way Interactions	3	21507	21507	7169	*	*
Diameter*Length	1	18106	18106	18106	*	*
Diameter*Velocity	1	126	126	126	*	*
Length*Velocity	1	3275	3275	3275	*	*
3-Way Interactions	1	46	46	46	*	*
Diameter*Length*Velocity	1	46	46	46	*	*
Residual Error	0	*	*	*		
Total	7	242089				

Factorial Fit: Biomass Slag Bat versus Diameter, Length, Velocity

Estimated Effects and Coefficients for Biomass Slag Bath Temperature (coded units)

Term	Effect	Coef	SE Coef	T	P
Constant		1866.94	11.98	155.80	0.000
Diameter	-168.81	-84.40	11.98	-7.04	0.006
Length	276.76	138.38	11.98	11.55	0.001
Velocity	-71.95	-35.98	11.98	-3.00	0.058
Diameter*Length	-95.15	-47.57	11.98	-3.97	0.029

S = 33.8936 PRESS = 24507.3

R-Sq = 98.58% R-Sq(pred) = 89.88% R-Sq(adj) = 96.68%

Analysis of Variance for Biomass Slag Bath Temperature (coded units)

Source	DF	Seq SS	Adj SS	Adj MS	F	P
Main Effects	3	220536	220536	73512	63.99	0.003
Diameter	1	56993	56993	56993	49.61	0.006
Length	1	153189	153189	153189	133.35	0.001
Velocity	1	10354	10354	10354	9.01	0.058
2-Way Interactions	1	18106	18106	18106	15.76	0.029
Diameter*Length	1	18106	18106	18106	15.76	0.029
Residual Error	3	3446	3446	1149		
Total	7	242089				

Response Optimization

Parameters

	Goal	Lower Target	Upper Target	Weight	Import
Biomass Slag	Target	1682	1701	2195	10 1

Global Solution

Diameter = 2.5
 Length = 6
 Velocity = 3.87101

Predicted Responses

Biomass Slag = 1701.13 , desirability = 0.997472

Composite Desirability = 0.997472

Factorial Fit: MSW Slag Bath Te versus Diameter, Length, Velocity

Estimated Effects and Coefficients for MSW Slag Bath Temperature (coded units)

Term	Effect	Coef
Constant		2675.6
Diameter	-583.3	-291.7
Length	439.2	219.6
Velocity	-212.9	-106.5
Diameter*Length	-350.5	-175.2
Diameter*Velocity	9.1	4.5
Length*Velocity	-91.5	-45.7
Diameter*Length*Velocity	-1.8	-0.9

Analysis of Variance for MSW Slag Bath Temperature (coded units)

Source	DF	Seq SS	Adj SS	Adj MS	F	P
Main Effects	3	1157076	1157076	385692	*	*
Diameter	1	680583	680583	680583	*	*
Length	1	385811	385811	385811	*	*
Velocity	1	90683	90683	90683	*	*
2-Way Interactions	3	262565	262565	87522	*	*
Diameter*Length	1	245665	245665	245665	*	*
Diameter*Velocity	1	164	164	164	*	*
Length*Velocity	1	16735	16735	16735	*	*
3-Way Interactions	1	6	6	6	*	*
Diameter*Length*Velocity	1	6	6	6	*	*
Residual Error	0	*	*	*		
Total	7	1419648				

Factorial Fit: MSW Slag Bath Te versus Diameter, Length, Velocity

Estimated Effects and Coefficients for MSW Slag Bath Temperature (coded units)

Term	Effect	Coef	SE Coef	T	P
Constant		2675.6	3.266	819.27	0.000
Diameter	-583.3	-291.7	3.266	-89.31	0.000
Length	439.2	219.6	3.266	67.24	0.000
Velocity	-212.9	-106.5	3.266	-32.60	0.001
Diameter*Length	-350.5	-175.2	3.266	-53.66	0.000
Length*Velocity	-91.5	-45.7	3.266	-14.00	0.005

S = 9.23708 PRESS = 2730.36

R-Sq = 99.99% R-Sq(pred) = 99.81% R-Sq(adj) = 99.96%

Analysis of Variance for MSW Slag Bath Temperature (coded units)

Source	DF	Seq SS	Adj SS	Adj MS	F	P
Main Effects	3	1157076	1157076	385692	4520.34	0.000
Diameter	1	680583	680583	680583	7976.49	0.000
Length	1	385811	385811	385811	4521.74	0.000
Velocity	1	90683	90683	90683	1062.81	0.001
2-Way Interactions	2	262401	262401	131200	1537.68	0.001
Diameter*Length	1	245665	245665	245665	2879.22	0.000
Length*Velocity	1	16735	16735	16735	196.14	0.005
Residual Error	2	171	171	85		
Total	7	1419648				

Response Optimization

Parameters

	Goal	Lower Target	Upper Target	Weight	Import
MSW Slag Bat	Target	2284	2395	3517	10

Global Solution

Diameter = 2.5
 Length = 6
 Velocity = 3.33040

Predicted Responses

MSW Slag Bat = 2395.35 , desirability = 0.996863

Composite Desirability = 0.996863

Factorial Fit: Coal Slag Bath T versus Diameter, Length, Velocity

Estimated Effects and Coefficients for Coal Slag Bath Temperature (coded units)

Term	Effect	Coef
Constant		2559.0
Diameter	-525.5	-262.7
Length	383.9	192.0
Velocity	-206.5	-103.2
Diameter*Length	-344.3	-172.2
Diameter*Velocity	47.4	23.7
Length*Velocity	-92.2	-46.1
Diameter*Length*Velocity	33.7	16.9

Analysis of Variance for Coal Slag Bath Temperature (coded units)

Source	DF	Seq SS	Adj SS	Adj MS	F	P
Main Effects	3	932277	932277	310759	*	*
Diameter	1	552216	552216	552216	*	*
Length	1	294797	294797	294797	*	*
Velocity	1	85264	85264	85264	*	*
2-Way Interactions	3	258643	258643	86214	*	*
Diameter*Length	1	237140	237140	237140	*	*
Diameter*Velocity	1	4499	4499	4499	*	*
Length*Velocity	1	17004	17004	17004	*	*
3-Way Interactions	1	2273	2273	2273	*	*
Diameter*Length*Velocity	1	2273	2273	2273	*	*
Residual Error	0	*	*	*		
Total	7	1193193				

Factorial Fit: Coal Slag Bath T versus Diameter, Length, Velocity

Estimated Effects and Coefficients for Coal Slag Bath Temperature (coded units)

Term	Effect	Coef	SE Coef	T	P
Constant		2559.0	31.47	81.31	0.000
Diameter	-525.5	-262.7	31.47	-8.35	0.004
Length	383.9	192.0	31.47	6.10	0.009
Velocity	-206.5	-103.2	31.47	-3.28	0.046
Diameter*Length	-344.3	-172.2	31.47	-5.47	0.012

S = 89.0233 PRESS = 169070

R-Sq = 98.01% R-Sq(pred) = 85.83% R-Sq(adj) = 95.35%

Analysis of Variance for Coal Slag Bath Temperature (coded units)

Source	DF	Seq SS	Adj SS	Adj MS	F	P
Main Effects	3	932277	932277	310759	39.21	0.007
Diameter	1	552216	552216	552216	69.68	0.004
Length	1	294797	294797	294797	37.20	0.009
Velocity	1	85264	85264	85264	10.76	0.046
2-Way Interactions	1	237140	237140	237140	29.92	0.012
Diameter*Length	1	237140	237140	237140	29.92	0.012
Residual Error	3	23775	23775	7925		
Total	7	1193193				

Response Optimization

Parameters

	Goal	Lower	Target	Upper	Weight	Import
Coal Slag Ba	Target	2226	2327	3375	10	1

Global Solution

Diameter = 2.5
Length = 6
Velocity = 5.22253

Predicted Responses

Coal Slag Ba = 2327.61 , desirability = 0.994172

Composite Desirability = 0.994172

Appendix E

Auxiliary Heating Cost Calculation for Various Feedstocks

The cost of the auxiliary heating of the slag bath was based on the optimized slag bath temperature determined in ANSYS Fluent for each slag material, and the following reactor temperatures: 996 K for biomass (Klass 1998), 1598 K for MSW (Gang et al. 2007), and 1201 K for coal (Klass 1998).

The following assumptions were made:

1. The tank had a 5 meter diameter and 5 meter height which would hold 1.5 days total slag discharge from a gasifier with 7.5 tons/hr slag production
2. The tank was maintained with a volume of 2/3 the total tank volume
3. The tank sides would have a similar heat transfer coefficient to the value calculated in Appendix C
4. The density and specific heat were estimated using the dominant species constituting the slag
5. Heat loss from the top of the tank is negligible as the top of the tank is receiving heat from the reactor
6. The tank is only started up once a year and is running 24 hours a day, 365 days a year with an availability of 90 percent
7. The auxiliary heat is provided through natural gas at a cost of 4 \$/MBtu

The following equation was used to determine the heating of the liquid slag at startup

$$Q_{heat} = mc_p \Delta T$$

Where m is the mass (kilograms), c_p is the specific heat (kilojoules/kg*K), and ΔT is the temperature difference between the liquid slag and the temperature of the reactor.

The equation for the heat loss from the sides and bottom of the tank was expressed as

$$Q_{loss\ sides} = \frac{UA\Delta T_M}{1000} * t$$

Where U is the heat transfer coefficient (W/m*K), A is the surface area of the tanks sides and bottom (m^2), ΔT_M is the mean temperature difference between atmospheric air and the liquid slag, and t is the time the slag bath is running.

The auxiliary heating cost was then found by combining the two equations for heat requirements for startup and heat loss during operation.

The following table was formulated in Microsoft Excel for optimized auxiliary heating cost.

Auxiliary Heating Cost With Optimized Design					
	Diameter (m)	5			
	Height (m)	5			
	Volume (m ³)	98.17477			
	Liquid Volume (m ³)	65.44985			
	Tank Surface Area (m ²)	98.17477			
Density (kg/m ³)	Biomass	2390	ΔT	Biomass	705
	MSW	2211		MSW	796
	Coal	2211		Coal	1126
Mass (kg)	Biomass	156425.1	ΔT_M	Biomass	999.5
	MSW	144709.6		MSW	1346
	Coal	144709.6		Coal	1312.5
Cp (kJ/kg*K)	Biomass	0.454	Q_{heat} (MBtu)	Biomass	47.46629
	MSW	0.074		MSW	8.081202
	Coal	0.074		Coal	11.43145
Temperature of Reactor (K)	Biomass	996	Q_{loss} sides (MBtu)	Biomass	19802.81
	MSW	1598		MSW	27094.61
	Coal	1201		Coal	26385.59
Temperature of Slag (K)	Biomass	1701	Heat Cost (\$)	Biomass	79401.11
	MSW	2394		MSW	108410.7
	Coal	2327		Coal	105588.1
U (W/m ² *K)	Biomass	7.5			
	MSW	7.62			
	Coal	7.61			

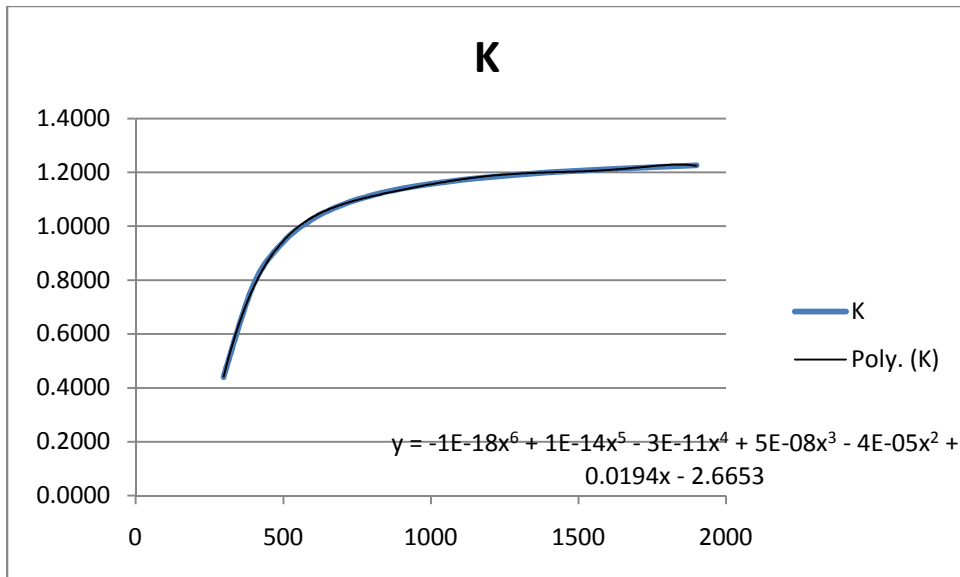
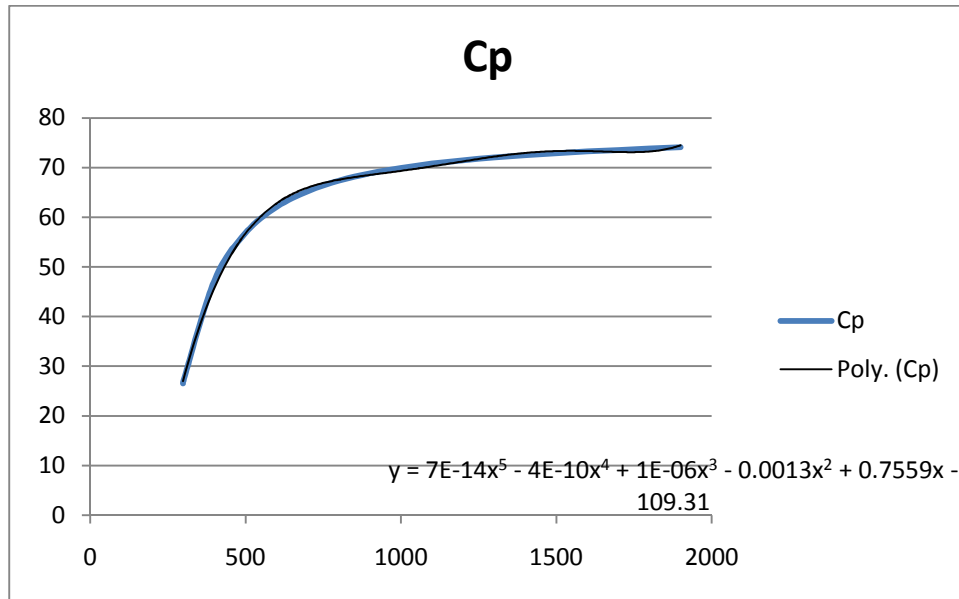
Then the auxiliary heating cost for a non-optimized system was analyzed, assuming the highest slag bath temperature for each respective material determined from ANSYS Fluent in Table 5.

Auxiliary Heating Cost Without Optimized Design					
	Diameter (m)	5			
	Height (m)	5			
	Volume (m ³)	98.17477			
	Liquid Volume (m ³)	65.44985			
	Tank Surface Area (m ²)	98.17477			
Density (kg/m ³)	Biomass	2390	ΔT	Biomass	1199
	MSW	2211		MSW	1920
	Coal	2211		Coal	2174
Mass (kg)	Biomass	156425.1	ΔT_M	Biomass	1246.5
	MSW	144709.6		MSW	1908
	Coal	144709.6		Coal	1836.5
Cp (kJ/kg*K)	Biomass	0.454	Q_{heat} (MBtu)	Biomass	80.72636
	MSW	0.074		MSW	19.49235
	Coal	0.074		Coal	22.07102
Temperature of Reactor (K)	Biomass	996	$Q_{loss\ sides}$ (MBtu)	Biomass	24696.55
	MSW	1598		MSW	38407.51
	Coal	1201		Coal	36919.72
Temperature of Slag (K)	Biomass	2195	Heat Cost (\$)	Biomass	99109.12
	MSW	3518		MSW	153708
	Coal	3375		Coal	147767.2
U (W/m ² *K)	Biomass	7.5			
	MSW	7.62			
	Coal	7.61			

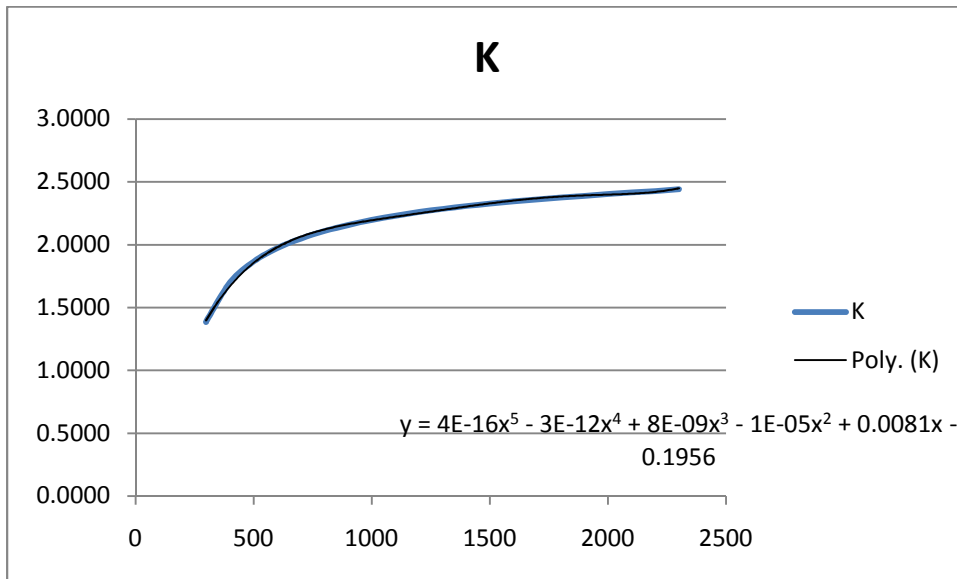
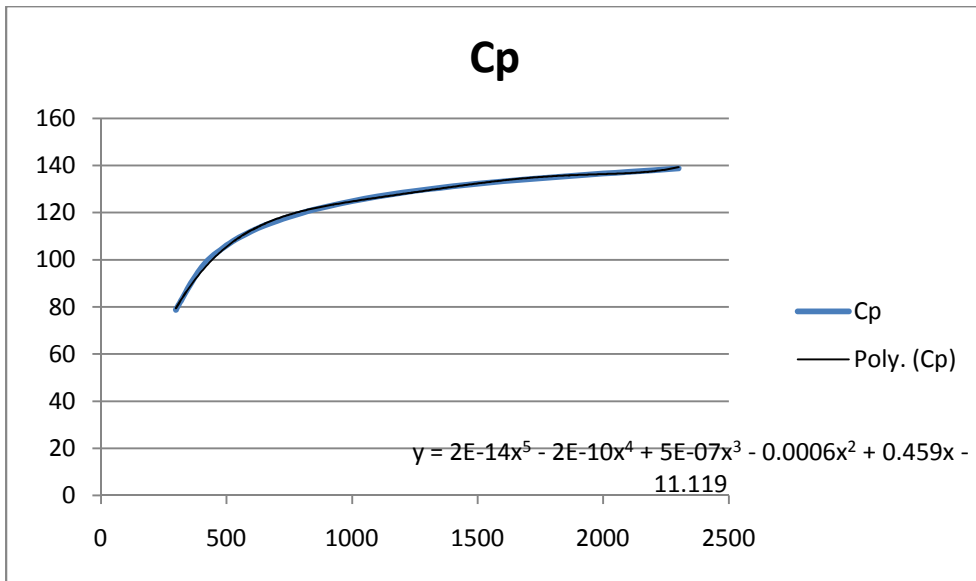
Appendix F

Polynomial Equations for Specific Heat and Thermal Conductivity

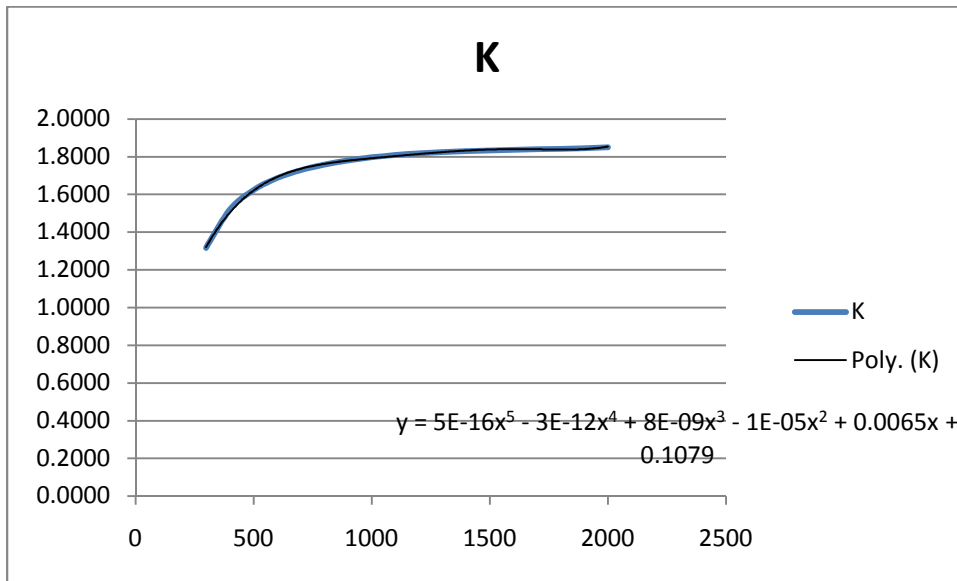
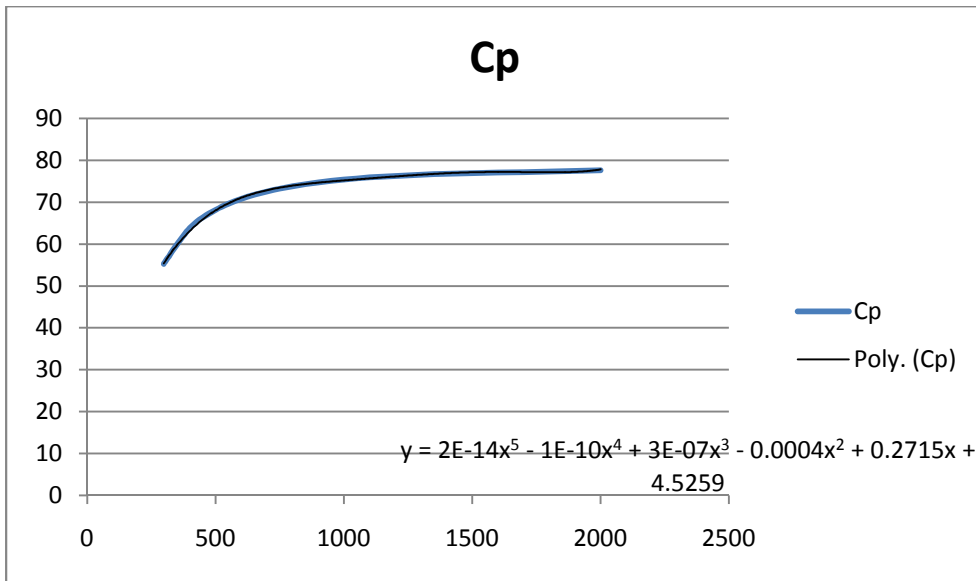
SiO₂



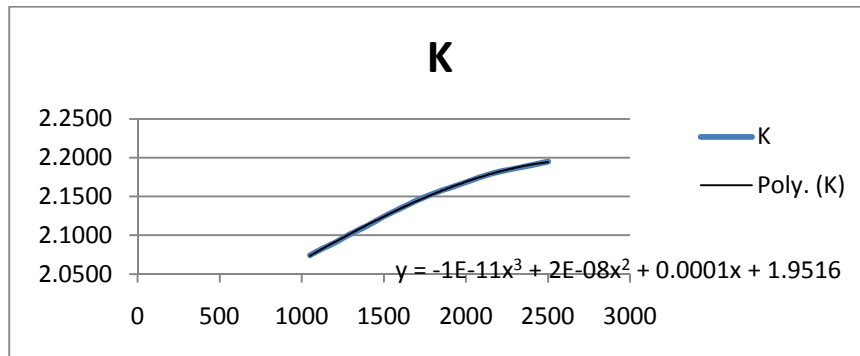
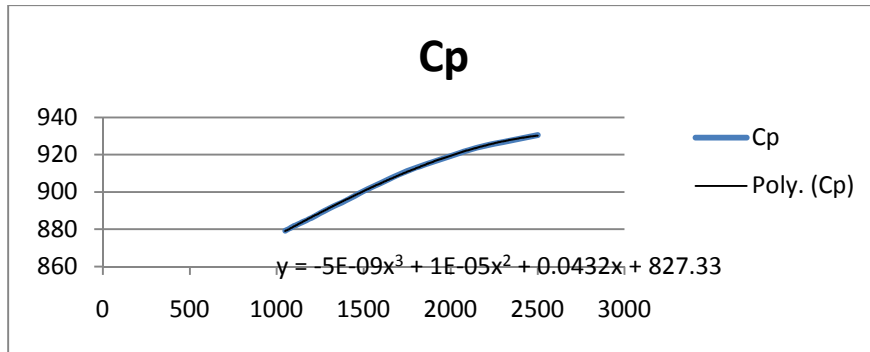
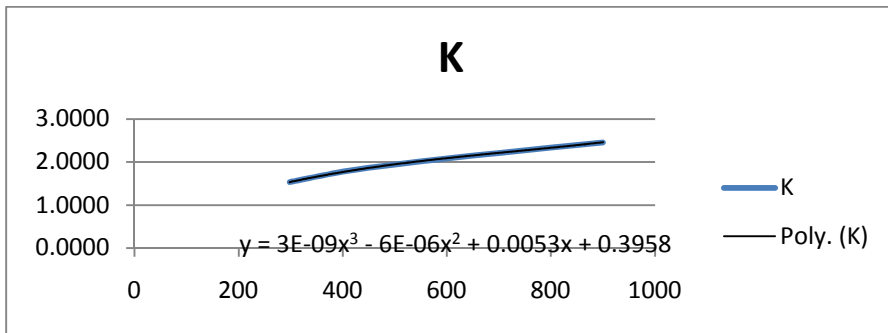
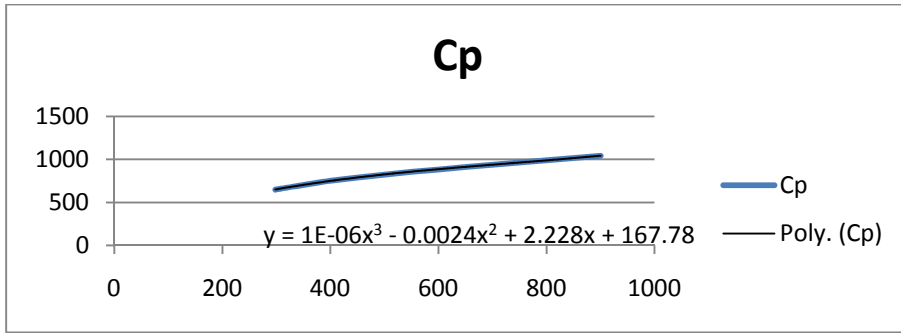
Al2O3



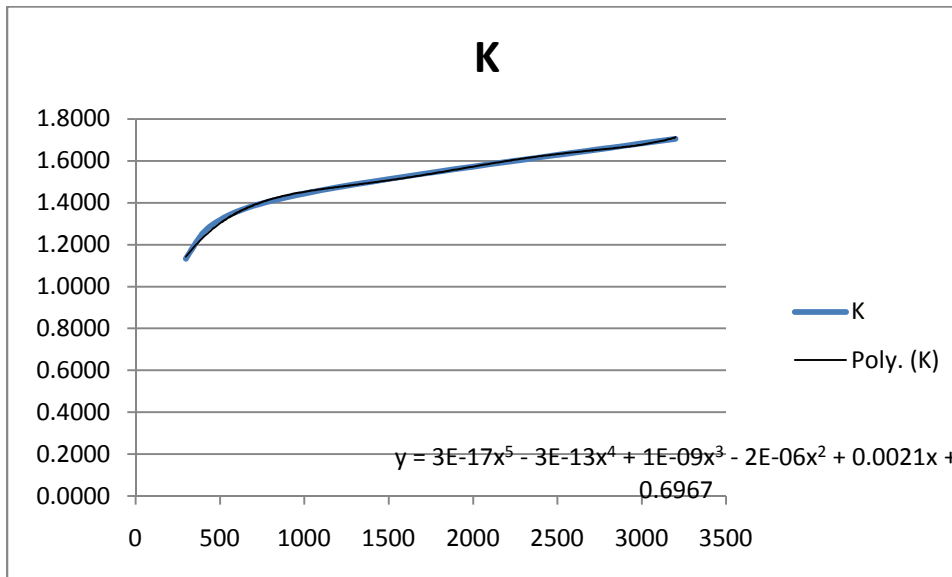
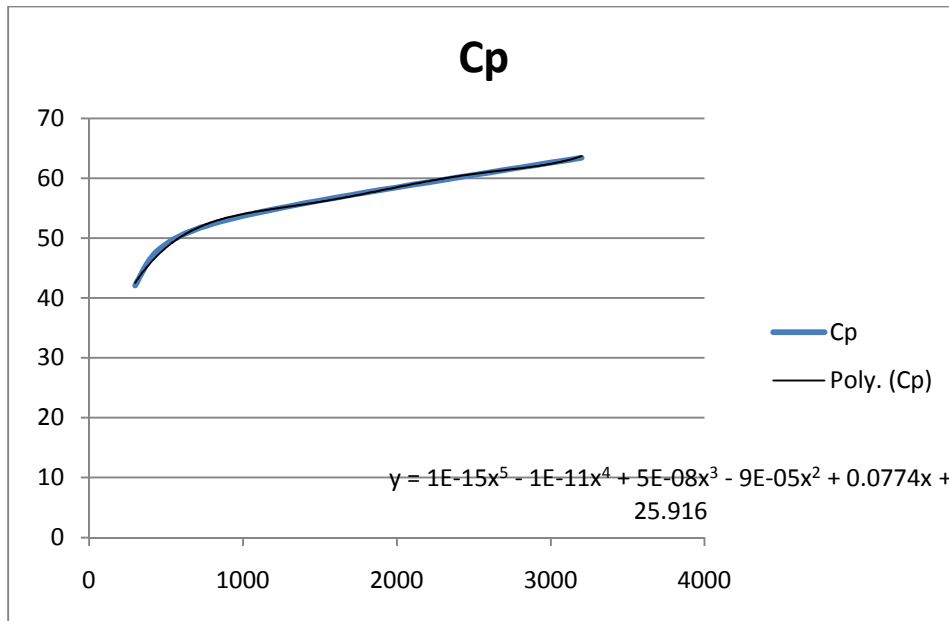
TiO2



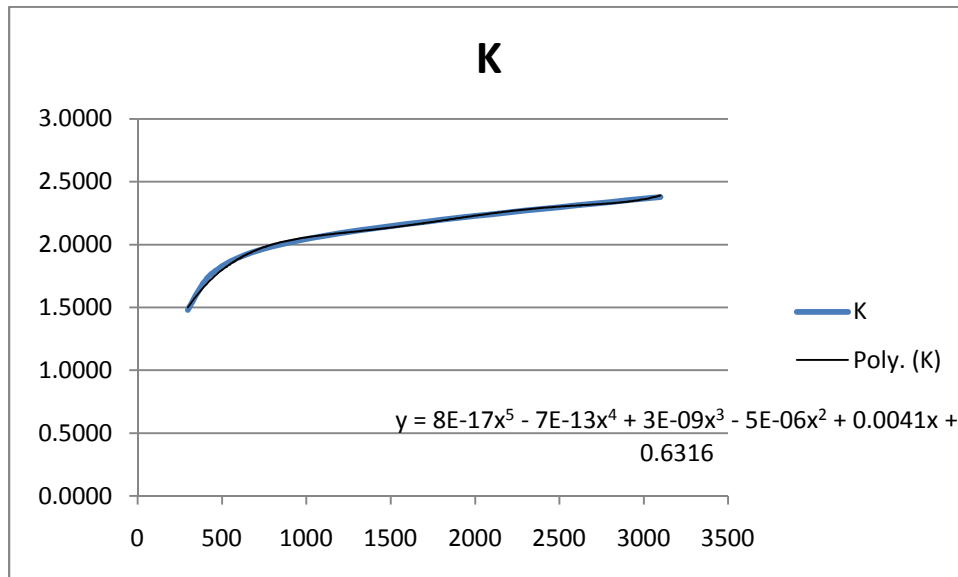
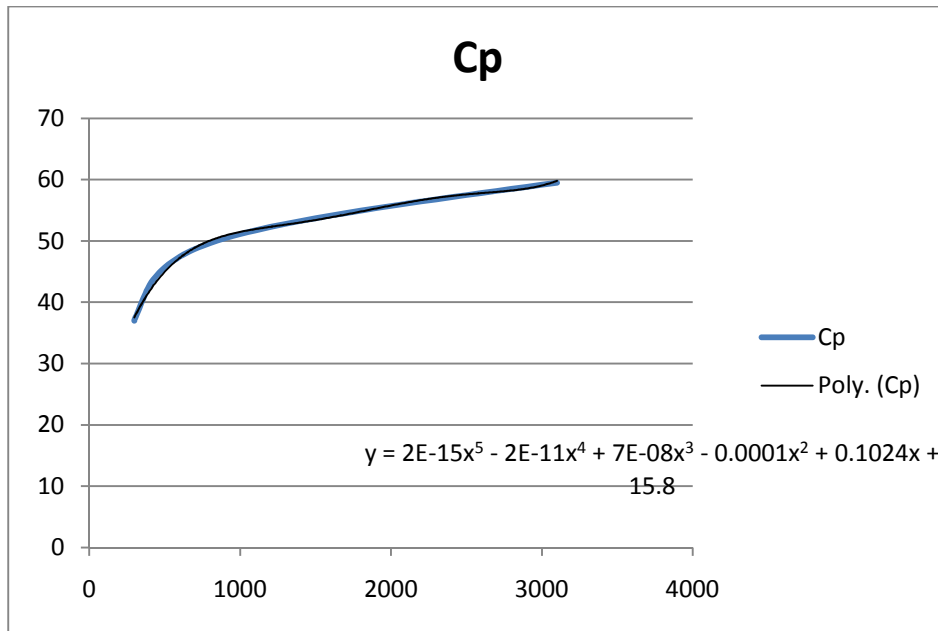
Fe2O3



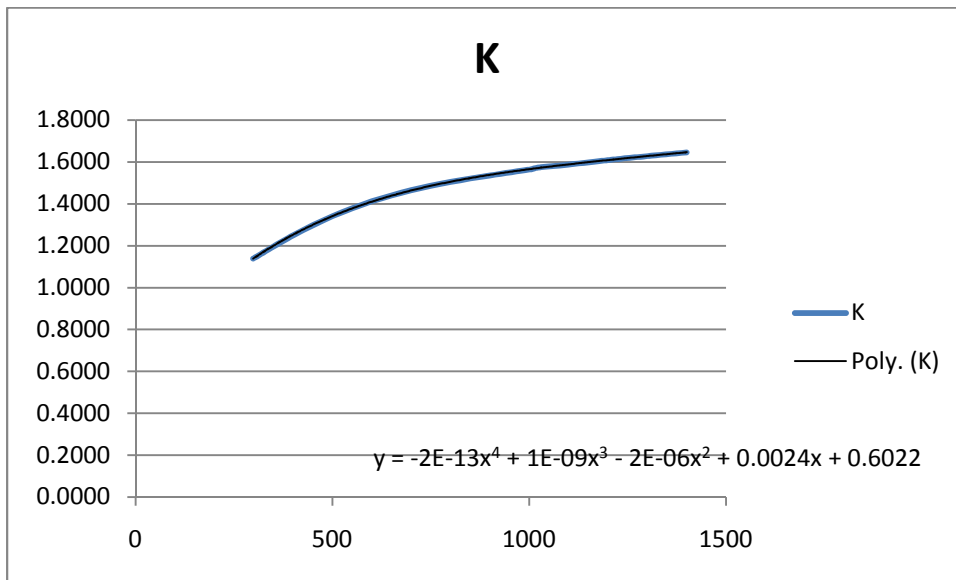
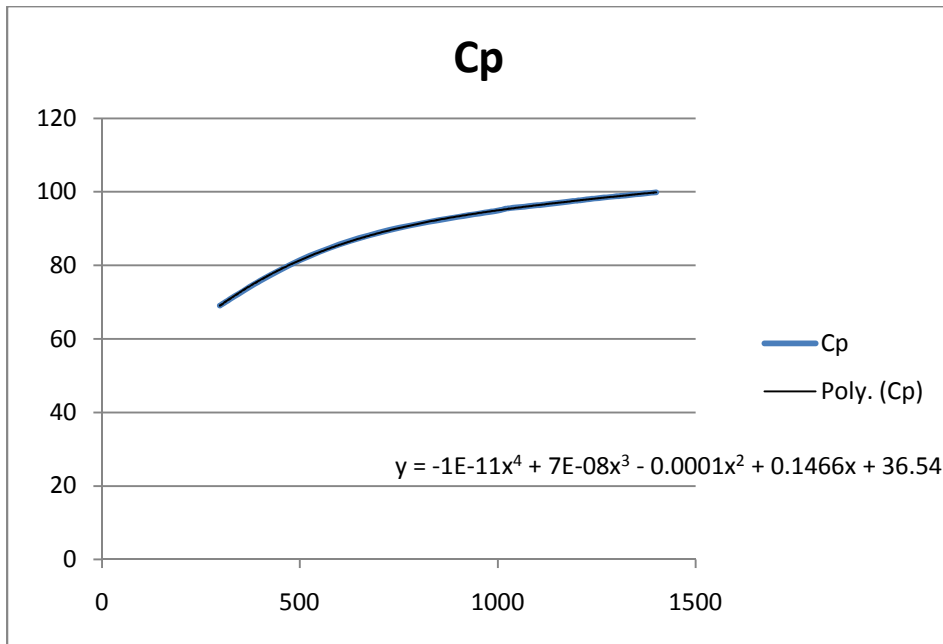
CaO



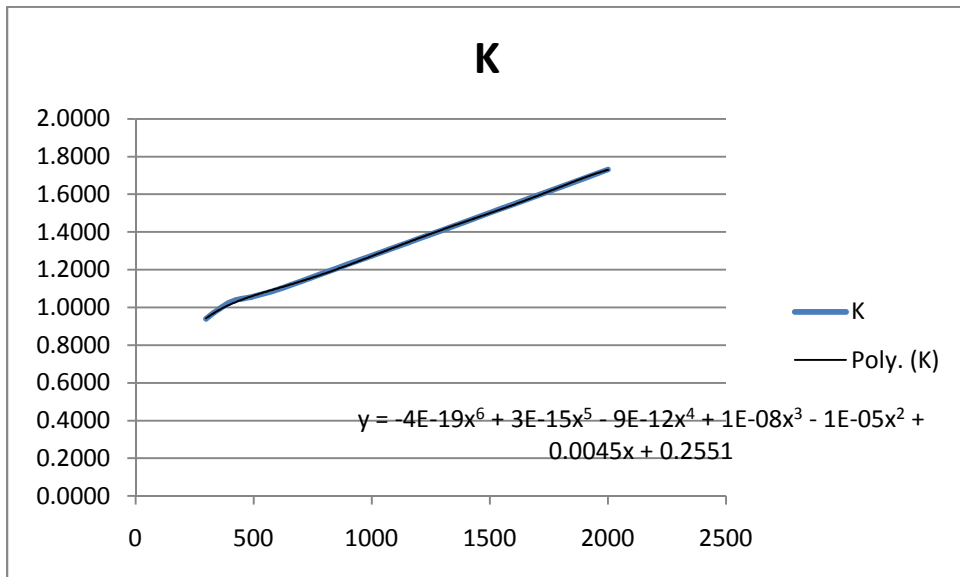
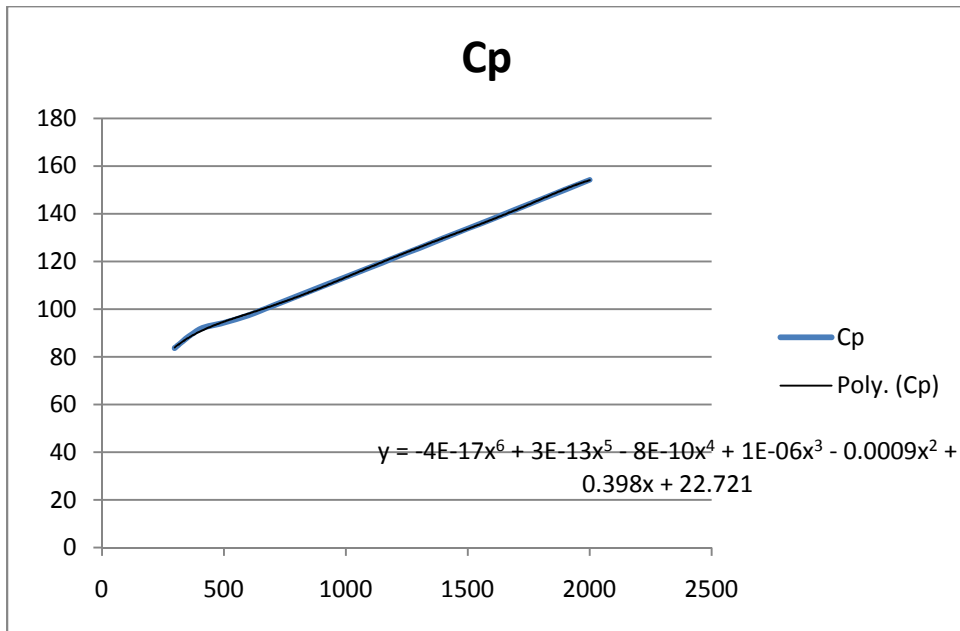
MgO



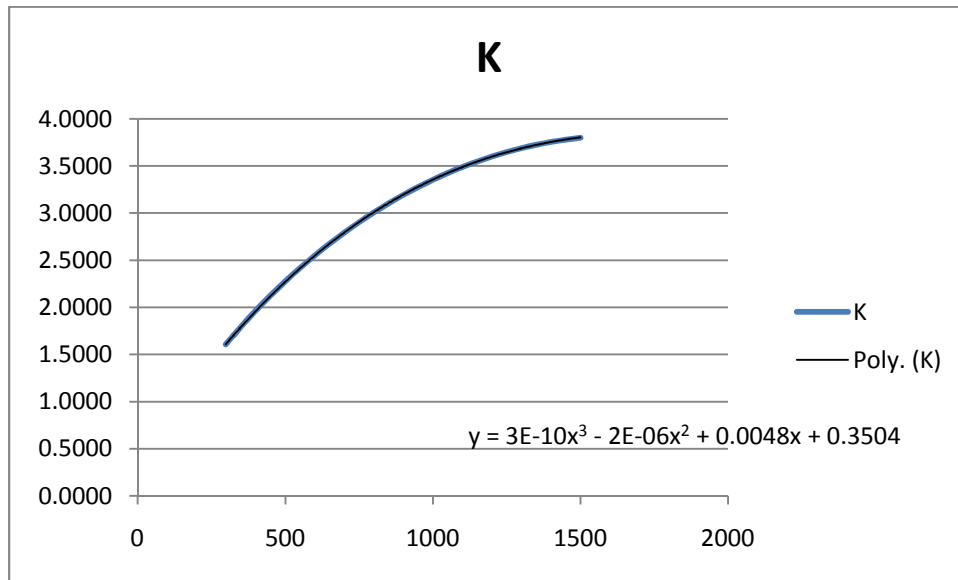
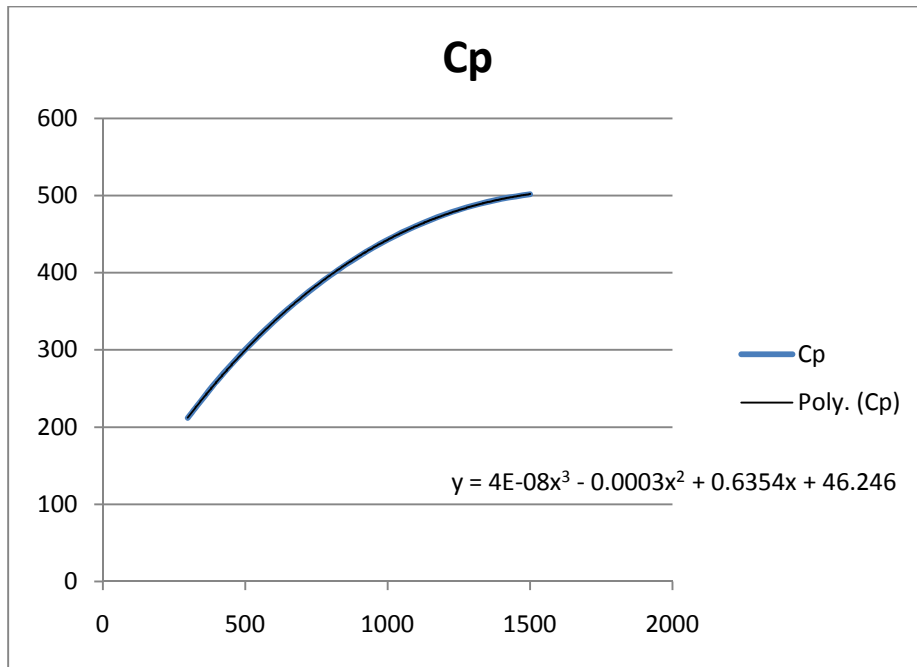
Na2O



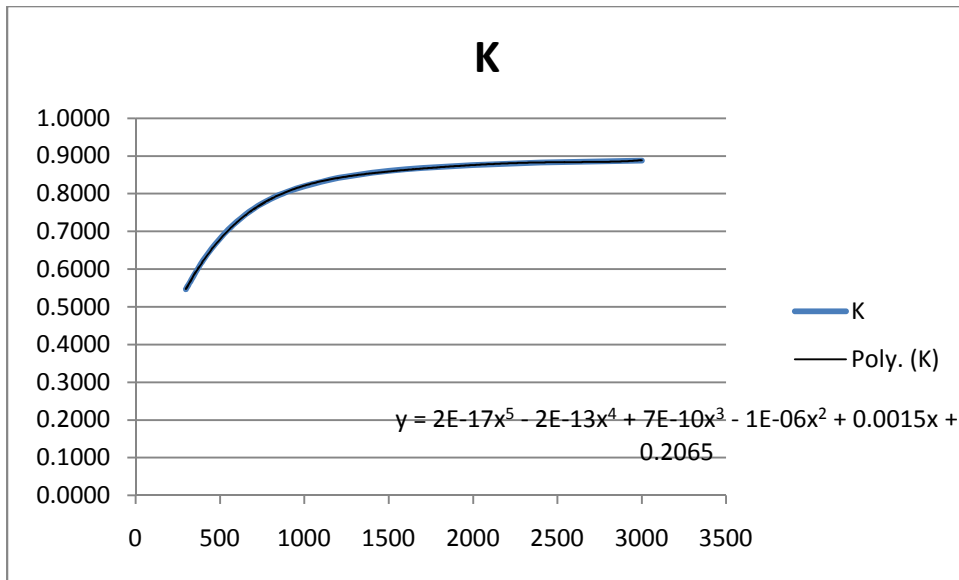
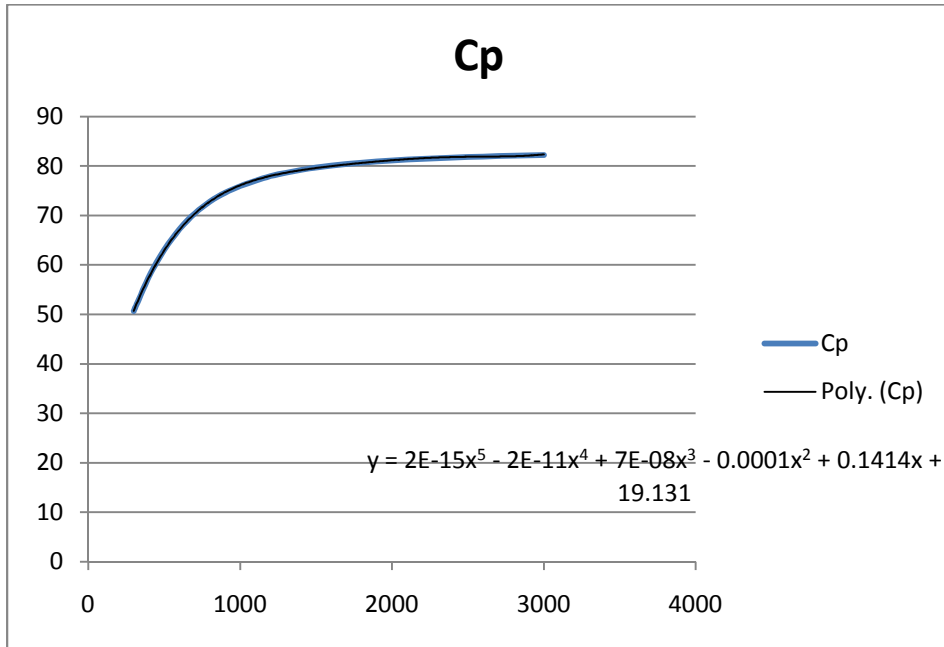
K2O



P2O5



SiO3



References

- Ashrafian, A. and S.T. Johansen (2006). "Tapping of Stratified Liquids from a Packed Bed." International Conference on CFD in the Process Industries, Melbourne, Australia.
- Blunk, S.L. and B.M. Jenkins (2000). "Combustion Properties of Lignin Residue from Lignocellulose Fermentation." Davis, California, University of California Davis.
- Buttke, B., R. Giering, U. Schlotter, B. Himmelreich, and K. Wittstock (2005). "Full Scale Industrial Recovery Trials for Shredder Residue in a High Temperature Slagging Bed Gasifier in Germany." Brussels, Belgium, Plastics Europe.
- Department of Trade and Industry. (1998). "Gasification of Solid and Liquid Fuels for Power Generation."
- Featherston, D. (2003). "Copper Smelter Tapping Block Design." San Francisco, CA, Synergetics Environmental Engineering.
- Higman, C. and M. Van der Burgt (2003). Gasification. Gulf Professional Publishing, Massachusetts.
- Ilyushechkin, A.Y., S.S. Hla, D.G. Roberts, and N.N. Kinaev (2010). "The Effect of Solids and Phase Compositions on Viscosity behavior and Tcv of Slags from Australian Bituminous Coals." Journal of Non-Crystalline Solids **357**: 893-902.
- Incropera, F.P and D.P. DeWitt (2001). Introduction to Heat Transfer. John Wiley & Sons, Inc, Massachusetts.
- Koukouza, N., A. Katsiadakis, E. Karlopoulos, and E. Kakaras (2008). "Co-Gasification of Solid Waste and Lignite – A Case Study for Western Macedonia." Waste Management **28**: 1263-1275.
- Lide, D.R. (2005). CRC Handbook of Chemistry and Physics. Chemical Rubber Publishing Company, Florida.
- Lin, W., Q. Liang, G. Yu, H. Liu, and X. Gong (2011). "Numerical Modeling for Non-Steady Thermal Stress Analysis of Slag Layer in a Membrane Wall Entrained-Flow Gasifier." Fuel **90**: 2396-2403.
- Mills, K.C. (2011). "The Estimation of Slag Properties." International Conference of Southern African Pyrometallurgy, Cradle of Humankind, South Africa.

- Mills, K.C. and J.M. Rhine (1989). "The Measurement and Estimation of the Physical Properties of Slags Formed During Coal Gasification." Fuel **68**: 904-911.
- Van Der Drift, A., H. Boerrigter, B. Coda, M.K. Cieplik, and K. Hemmes (2003). "Entrained Flow Gasification of Biomass – Ash Behavior, Feeding Issues, and System Analyses." Petten, The Netherlands, ECN Energy Solutions.
- Vargas, S., F.J. Frandsen, and K. Dam-Johansen (2000). "Rheological Properties of High-Temperature Melts of Coal Ashes and Other Silicates." Progress in Energy and Combustion Science **27**: 237-429.
- Wang, T. and A. Silaen (2007). "Effect of Slag Tap Size on Gasification Performance and Heat Losses in a Quench-Type Coal Gasifier." International Pittsburgh Coal Conference, Johannesburg, South Africa.
- Zhan, Z., Y. Xiao, Y. Yang, R. Boom, and J. Voncken (2009). "Vitrified Bottom Ash Slag from Municipal Solid Waste Incinerators – Phase Relations of CaO-SiO₂-Na₂O Oxide System." Molten: 43-50.

Vita

Noah Avram Meltz Weichselbaum was born November 21, 1982 in Seoul, South Korea. He was adopted by his parents Paul and Elyse when still only a few months old. He was raised in Syracuse, New York, where he attended William Nottingham High School graduating in 2001.

He received a presidential scholarship to attend Union College in Schenectady, NY where he studied mechanical engineering. While there he ran cross-country and track at the division three level, and was inducted into Pi Tau Sigma and the Order of the Engineer. He worked as a research assistant to Professor Frank Wicks during the summer of 2005 researching and testing ultra-capacitors. He graduated in the spring of 2006 with a Bachelor of Science Degree in Mechanical Engineering.

Following graduation he worked for Lockheed Martin Systems Integration in Owego, New York where he worked on the Presidential Helicopter program. During this time he became engaged to his fiancée Natasha, with whom he moved in the summer of 2008 to Kansas City so she could attend school at the University of Kansas to pursue her medical degree. He went to work for Smith and Loveless in Lenexa, Kansas, and enrolled at the University of Kansas City Missouri in the fall of 2009.

In the spring of 2011 he began research under the guidance of Professor Anthony Black on his thesis for the completion of his Master of Science degree in Mechanical Engineering. Following graduation in the winter of 2011 he plans to

pursue a doctoral degree in Mechanical Engineering continuing research in thermal fluids.